Robust IL-2-dependent antitumor immunotherapy requires targeting the high-affinity IL-2R on tumor-specific CD8+ T cells

Kathryn M LaPorte, Rosmely Hernandez, Alicia Santos Savio, Thomas R Malek

Department of Microbiology and Immunology, University of Miami Miller School of Medicine, Miami, Florida, USA

Correspondence to
Dr Thomas R Malek;
tmalek@med.miami.edu

ABSTRACT

Background Development of interleukin (IL)-2-dependent antitumor responses focus on targeting the intermediate affinity IL-2R to stimulate memory-phenotypic CD8+ T and natural killer (NK) cells while minimizing regulatory T cell (Treg) expansion. However, this approach may not effectively engage tumor-specific T effector cells. Since tumor-antigen specific T cells upregulate the high-affinity IL-2R, we tested an IL-2 biologic, mouse IL-2/CD25, with selectivity toward the high-affinity IL-2R to support antitumor responses to tumors that vary in their immunogenicity.

Methods Mice were first implanted with either CT26, MC38, B16.F10, or 4T1 and after a tumor mass developed, they were treated with high-dose (HD) mouse (m)IL-2/CD25 alone or in combination with anti-programmed cell death protein-1 (PD-1) checkpoint blockade. Tumor growth was monitored and in parallel the immune signature in the tumor microenvironment (TME) was determined by a combination of multiparameter flow cytometry, functional assays, and enumeration of tumor-reactive T cells.

Results We show that HD mIL-2/CD25, which preferentially stimulates the high-affinity IL-2R, but not IL-2/anti-IL-2 complexes with preferential activity toward the intermediate-affinity IL-2R, supports vigorous antitumor responses to immunogenic tumors as a monotherapy that were enhanced when combined with anti-PD-1. Treatment of CT26-bearing mice with HD mIL-2/CD25 led to a high CD8+:Treg ratio in the TME, increased frequency and function of tumor-specific CD8+ T effector cells with a less exhausted phenotype, and antitumor memory responses.

Conclusions Targeting the high-affinity IL-2R on tumor-specific T cells with HD mIL-2/CD25 alone or with PD-1 blockade supports antitumor responses, where the resulting memory response may afford long-term protection against tumor re-emergence.

WHAT IS ALREADY KNOWN ON THIS TOPIC

⇒ Much emphasis in the field has been to use interleukin (IL)-2R agonists with selectivity toward the intermediate-affinity IL-2R to broadly expand CD8+ T and natural killer cells to enhance antitumor immune responses as this approach would limit expansion of immunosuppressive regulatory T cells (Tregs). Preclinical studies have shown that this approach leads to a reduction in tumor growth.

WHAT THIS STUDY ADDS

⇒ The current study using preclinical mouse models demonstrates that an IL-2R agonist, a mouse IL-2/CD25 fusion protein, with selectivity toward the high-affinity IL-2R that targets T effector cells, generated more robust antitumor responses as a monotherapy or in combination with anti-programmed cell death protein-1 (PD-1) checkpoint blockade than those supported by IL-2R agonists with selectivity toward the intermediate-affinity IL-2R. Unexpectedly, Tregs did not increase in the tumor microenvironment, although they substantially expanded in peripheral immune tissues.

HOW THIS STUDY MIGHT AFFECT RESEARCH, PRACTICE OR POLICY

⇒ The results from this study offer a new approach for future clinical testing to enhance antitumor immunity, particularly in the context of checkpoint blockade, where many patients do not exhibit a durable response.

INTRODUCTION

Interleukin (IL)-2 was the first Food and Drug Administration approved immunotherapy for use in patients with metastatic melanoma and renal cell carcinoma.[1 2] However, the use of recombinant IL-2 (Proleukin/aldesleukin) has been problematic due to low response rates, off-target effects, and severe dose-dependent toxicities. Due to its potent T-cell growth factor activity and ability to promote development and activity of cytotoxic T lymphocytes and natural killer (NK) cells, IL-2 has been re-engineered for cancer immunotherapy to increase its half-life, decrease its toxicity, and to drive selectivity toward memory-phenotypic (MP) CD8+ T and NK cells.[3 4] Since these cells express high amounts of the intermediate-affinity IL-2R, consisting of CD122 (IL-2Rβ) and CD132 (γc), one major strategy has been to derive IL-2 biologics with reduced or absent binding to CD25 (IL-2Rα), which is essential to form

the high-affinity IL-2R. The rationale behind these CD122/CD132-selective IL-2s is to promote antitumor immunity while reducing non-specific toxicities, such as vascular leak syndrome,[5] and by minimizing undesired immunosuppressive regulatory T cells (Tregs).

High-affinity IL-2R-selective compounds have also been formulated primarily for use at low doses to boost Tregs in the context of autoimmunity and inflammatory disorders.[6–8] This class of IL-2 analogs has not been extensively explored for anticancer effects due to the concern of increased off-target Tregs. In the context of cancer immunotherapy, these high-affinity IL-2R biologics are expected to also react with recently activated tumor antigen-specific CD4+ and CD8+ T effector (Teff) cells that have upregulated CD25 to express the high-affinity IL-2R. Whether such an effect on tumor-responsive Teff cells is diminished by an accompanying polyclonal increase in Tregs remains to be determined. In contrast, the ability of CD122/CD132-selective IL-2s to expand tumor-reactive T cells depends on their frequency within the MP CD8+ T-cell population. Another potential limitation of CD122/CD132-selective IL-2s is that tumor-reactive T cells may need to compete with the global response to the IL-2 agonist by MP CD8+ T cells. Furthermore, CD122/CD132-selective IL-2s may not optimally stimulate tumor-reactive CD4+ T cells, as these are not characterized by expression of the intermediate affinity IL-2R,[9] yet these are increasingly appreciated to significantly contribute to antitumor responses.[10 11]

We have developed an IL-2 fusion protein comprised of mouse IL-2 and mouse CD25 (mIL-2/CD25) that has a longer half-life than IL-2 and preferentially targets cells that express the high-affinity IL-2R.[12] The selectivity toward high-affinity IL-2R stems from its unique mechanism of action, whereby mIL-2/CD25 predominantly forms biologically inactive head-to-tail transdimers that slowly dissociate into low concentrations of active mIL-2/CD25 monomers that readily stimulate cells bearing the high-affinity IL-2R. In practical terms, mIL-2/CD25 provides a continuous source of an IL-2 agonist which at low doses, selectively targets Tregs to limit autoimmunity[13] and at higher doses, also stimulates Teff cells with minimal stimulation of MP CD8+ T and NK cells. In previous tumor immunotherapy studies, we showed that the transient application of HD mIL-2/CD25 in the context of tumor neoantigen peptide-based vaccines readily supported antitumor immunity to the poorly immunogenic B16.F10 melanoma,[14 15] validating the application of this IL-2R agonist for cancer immunotherapy.

In this study, we tested the effectiveness of HD mIL-2/CD25 monotherapy or with anti-PD-1 checkpoint blockade to limit the growth of immunogenic tumors. When compared with IL-2/anti-IL-2 immune-complexes (IL2/IC) directed toward the intermediate-affinity IL-2R, HD mIL-2/CD25 monotherapy more effectively supported antitumor responses, with optimal tumor-free survival when co-administered with anti-PD-1. HD mIL2/CD25

enhanced the expansion of tumor-reactive T cells that showed a less exhausted phenotype and supported the development of an antitumor memory response. Thus, these preclinical studies support stimulating the high-affinity IL-2R in conjunction with checkpoint blockade to optimize antitumor activity.

RESULTS
HD mIL-2/CD25-induced antitumor activity correlates with tumor immunogenicity

Several mouse tumor models that vary in immunogenicity were used to test the efficacy of HD mIL-2/CD25 as a monotherapy. Tumor-bearing mice were treated biweekly for 2 weeks with mIL-2/CD25 (half-life of 16–18 hours) to maintain persistent IL-2R signaling. This treatment supported robust antitumor responses in mice bearing the highly immunogenic MC38 or CT26 colon carcinomas (figure 1A, online supplemental figure 1A,B). The mIL-2/CD25 exhibited less effective antitumor responses against the poorly immunogenic B16.F10 melanoma (figure 1A, online supplemental figure 1C) and was ineffective in mice bearing the non-immunogenic 4T1 mammary carcinoma (figure 1A, online supplemental figure 1D).

The mIL-2/CD25-treated mice that cleared CT26 were rechallenged with CT26 tumor cells approximately 3 months after the primary tumor was cleared. Compared with the rapid growth of CT26 in naïve mice, none of the 17 HD mIL-2/CD25-'cured' mice showed signs of tumor growth for 60 days post-tumor rechallenge (figure 1B, online supplemental figure 1E). After the rechallenge, an increase in AH1-specific CD8+ T cells, an immunodominant tumor antigen of CT26,[16 17] was noted when compared with naïve CT26-bearing mice (figure 1C). These data together suggest that persistent IL-2R signals expand pre-existing tumor-reactive Teff cells to effectively reject highly immunogenic tumors while supporting the development of an effective pool of tumor-reactive memory T cells.

Targeting the high-affinity IL-2R generates more effective antitumor responses than the intermediate-affinity IL-2R

Current IL-2-based approaches for antitumor immunity favor targeting the intermediate affinity IL-2R due to its selectivity toward MP CD8+ T and NK cells over Tregs.[3 4] To test the antitumor efficacy of IL-2 biologics with preferential activity toward the high-affinity versus intermediate-affinity IL-2R, HD mIL-2/CD25 was compared with IL-2Rβγ-directed IL-2/anti-IL-2 (S4B6) complexes, S4B6-IL2/IC. Consistent with other studies,[6 18–24] we also found that that a dose of 1.5 µg IL-2/15 µg S4B6 yielded substantial expansion of BALB/c and C57BL/6 CD8+ T and NK cells while exerting minimal effects on Tregs (online supplemental figure 2A), leading to optimal CD8+ T cell:Treg and NK:Treg ratios (online supplemental figure 2B). At the higher doses tested, this selectivity diminishes toward cells expressing only the intermediate-affinity
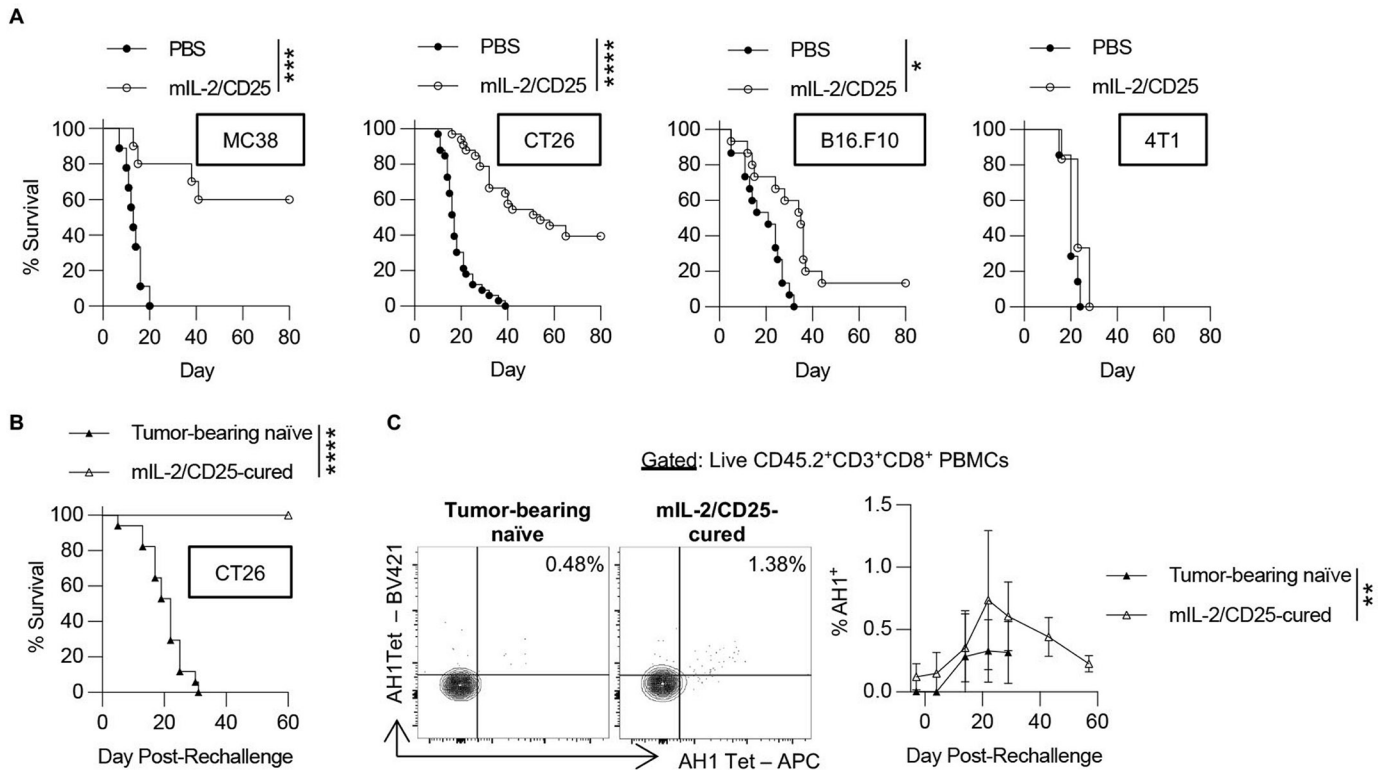
Figure 1 Immunogenic tumors are susceptible to HD mIL-2/CD25 therapy. (A) C57BL/6 mice bearing MC38 (n=9–10/group pooled from two experiments) or B16F10 (n=15/group pooled from three experiments) and BALB/c mice bearing CT26 (n=32–33/group pooled from five experiments) or (4T1 n=6–7/group pooled from two experiments) received PBS or HD mIL-2/CD25 (100 μg) two times a week for 10 (MC38) or 14 days (CT26, B16.F10, 4T1) and tumor growth was followed over time. Day 0 represents the start of administration of PBS or mIL-2/CD25. (B) CT26-bearing mice (n=17–18/group pooled from four experiments) treated with HD mIL-2/CD25 that showed tumor-free survival ('cured') were rechallenged with CT26 90 days post-tumor clearance. (C) AH1-tetramer$^+$ CD8$^+$ T cells were detected in the PBMCs (n=3–4/group) after rechallenge with CT26. Data is shown for D22 (representative flow plots, left; quantitative data, right). Survival data (A,B) were analyzed by a log-rank test. AH1 tetramer data (C) are shown as mean±SD and analyzed by a Welch's t-test of the area under the curve. HD, high-dose; mIL-2, mouse interleukin-2; PBS, phosphate-buffered saline; PBMCs, peripheral blood mononuclear cells.

IL-2R as Tregs increased. Thus, 1.5 μg IL-2 was complexed with 15 μg anti-IL-2 S4B6 for subsequent studies examining antitumor effects. In contrast, HD mIL-2/CD25 (100 μg) increased Tregs that express the high-affinity IL-2R but did not expand CD8$^+$ T cells or NK cells, which express high amounts of the intermediate-affinity IL-2R.

Mice bearing MC38, CT26, or B16.F10 received the IL-2 agonists for 2 weeks. As the half-life of S4B6-IL2/IC is shorter than mIL-2/CD25,[6 12 21 22] it was administered every other day to provide persistent IL-2Rβγ signaling in parallel to HD mIL-2/CD25. HD mIL-2/CD25 was more effective in supporting antitumor responses in each of these models (figure 2A). To verify the selectivity of the IL-2s during therapy, expansion of T and NK cells was assessed weekly in PBMCs. As expected, CD8$^+$ T cells and NK cells were readily expanded with S4B6-IL2/IC whereas Tregs were expanded with HD mIL-2/CD25 in CT26-bearing mice (figure 2B). Similar results were found for mice bearing MC38 and B16.F10 (online supplemental figure 3A,B). Importantly, these IL-2R agonists differentially supported CD8$^+$ T cell expansion in the TME, where greater expansion was found after treatment with HD mIL-2/CD25 (figure 2C). These data suggest that

the driver for the improved antitumor responses by HD mIL-2/CD25 is due to more effective accumulation of CD8$^+$ T cells in the TME when compared with S4B6-IL2/IC.

HD mIL-2/CD25 promotes antitumor responses by acting on pre-existing tumor-reactive CD8$^+$ T cells

To further evaluate the effect of HD mIL-2/CD25 monotherapy, the distribution of major T cell subsets was determined in the TME, spleen, and tumor-draining lymph node (TDLN) in CT26-bearing mice. In the TME, HD mIL-2/CD25 supported a substantial increase in frequency of CD3$^+$ T cells (figure 3A) and this was largely due to an increased frequency and number of CD8$^+$ T cells (figure 3B). The frequency of conventional CD4$^+$ Foxp3$^-$ T (Tconv) cells was low and unaffected and strikingly, the frequency of Tregs decreased (figure 3C). In contrast, the number of CD8$^+$ T cells in the spleen and TDLN were unchanged after HD mIL-2/CD25 (figure 3D); as expected, a large increase in Tregs was found in the spleen, with a much lesser effect in the TDLN (figure 3D). Targeting the high-affinity IL-2R with HD mIL2/CD25, therefore, selectively led to a very high
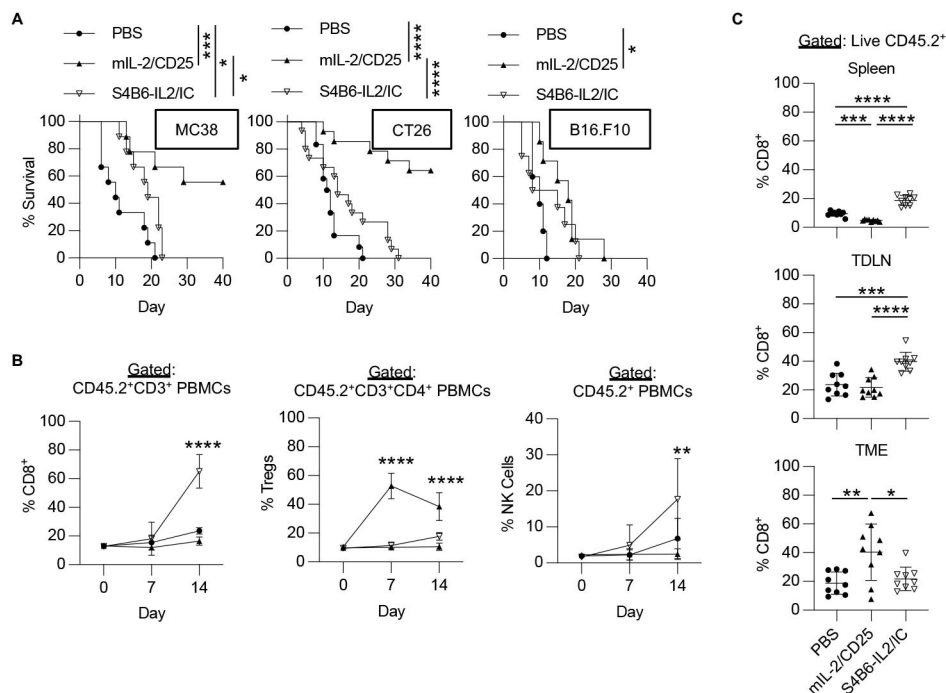
3

Figure 2 Targeting the high-affinity IL-2R with HD mIL-2/CD25 yields more productive antitumor responses than targeting the intermediate affinity IL-2R. (A) The indicated tumor-bearing mice (see legend to figure 1) received PBS, mIL-2/CD25 or S4B6-IL2/IC (1.5 µg mIL-2/15 µg S4B6); the latter was administered every other day for 12 (MC38, n=9/group pooled from two experiments) or 14 (CT26, 12–15/group pooled from three experiments; B16.F10, n=5–8/group pooled from two experiments) days. Mouse survival was assessed over time and analyzed by a log-rank test. (B) Frequencies of the indicated cells (n=10/group pooled from three experiments) for PBMCs collected from CT26-bearing mice. Data (mean±SD) were analyzed by the Kruskal-Wallis multiple comparison test. (C) CD8+ T cells from the indicated tissues were determined 7 days after initiation of the indicated treatments. Data (n=9/group pooled from three experiments) are shown as mean±SD and analyzed via one-way analysis of variance with Tukey's multiple comparison test. HD, high-dose; IC, immune-complexes; mIL-2, mouse interleukin-2; NK, natural killer; PBS, phosphate-buffered saline; PBMCs, peripheral blood mononuclear cells; TDLN, tumor-draining lymph node; TME, tumor microenvironment; Tregs, regulatory T cells.

CD8+ T cell to Treg ratio in the TME but not the spleen and TDLN (figure 3E). Overall, these data indicated that HD mIL-2/CD25 effectively supported the expansion of Tregs in secondary lymphoid tissues, but only CD8+ T cells showed expansion in the TME, leading to a high CD8+ T cell:Treg ratio, which is a good prognostic factor for antitumor responses.

To directly test that CD8+ T cells importantly contribute to the HD mIL-2/CD25-mediated antitumor response, CD8+ T cells were depleted prior to treatment with HD mIL-2/CD25. The effectiveness of CD8+ T cell depletion prior to and during treatment with HD IL-2/CD25 was verified for PBMCs (online supplemental figure 4A) for the same mice antitumor responses were evaluated. In the absence of CD8+ T cells, HD mIL-2/CD25-induced antitumor responses were completely abrogated (figure 3F, online supplemental figure 4B). These results indicate that CD8+ T cells are the major cellular driver of the antitumor activity induced by HD mIL-2/CD25.

Increased neutrophils in the TME by HD mIL-2/CD25 do not contribute to the anticancer response

The effect of HD-mIL-2/CD25 was also assessed for other cell types in the TME of CT26-bearing mice. We were particularly interested in dendritic cells (DCs) as

previous studies found that IL-2 and IL2/ICs indirectly activate and promote the expansion of type-I and type-II conventional DCs (cDC1s and cDC2s)[19 25 26] and in one study they confirmed that this occurred through FLT3L, CSF-2, and TNF and that the increase in DCs correlated with favorable anticancer responses.[26] The frequency (online supplemental figure 5A) and number (online supplemental figure 5B) of cDC1s and cDC2s as well as natural killer T (NKT) cells, and NK cells, was unchanged in the TME, where the latter result further demonstrates that HD mIL-2/CD25 is less effective in targeting the intermediate-affinity IL-2R. We do not know why we did not detect an increase in either cDC1 or cDC2 subsets but this may reflect some differences in the duration or cellular targeting of IL-2R signals by mIL-2/CD25.

A significant increase, however, was noted for neutrophils (online supplemental figure 5A,B). To assess whether this increase in neutrophils contributes to the antitumor response, anti-Ly6G was used to deplete these cells[27] prior to treatment of CT26-bearing mice with HD mIL-2/CD25. Examination of PBMCs revealed that anti-Ly6G effectively depleted neutrophils (online supplemental figure 6A). Nevertheless, the HD mIL-2/CD25-driven antitumor response to CT26 was largely
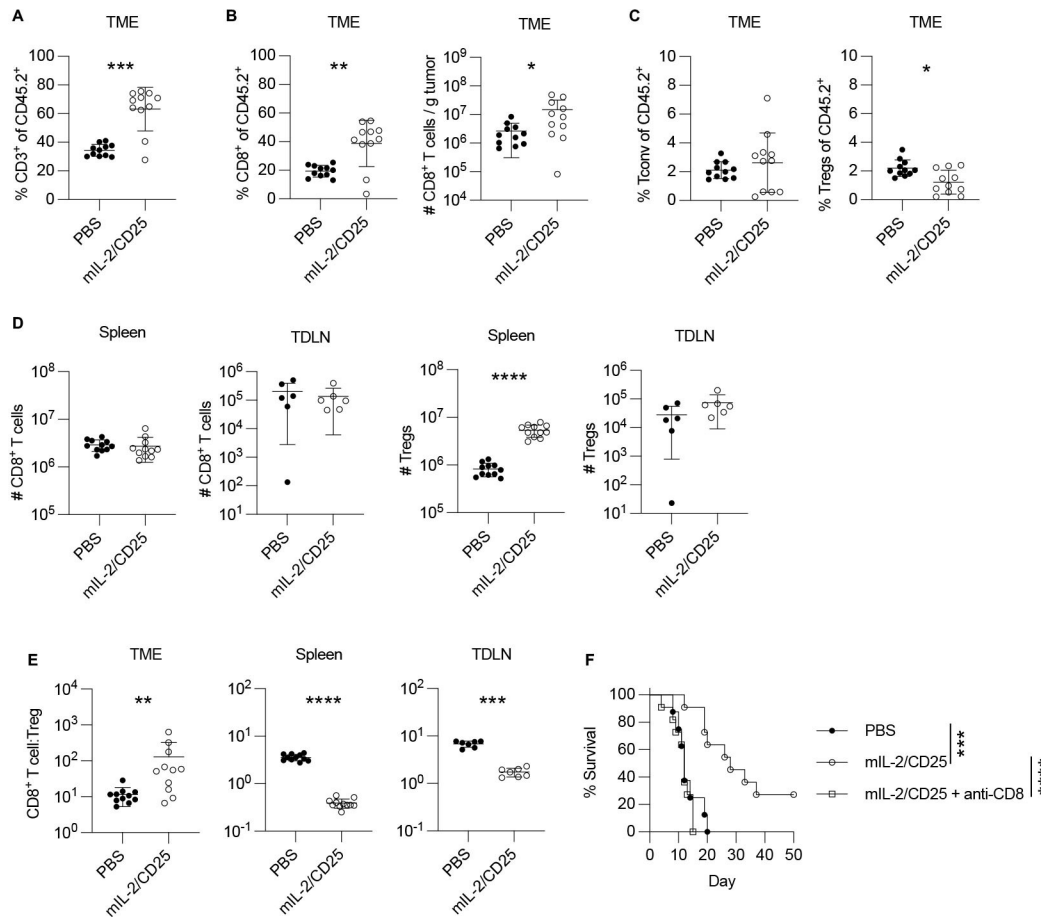
Figure 3 HD mIL-2/CD25-induced antitumor activity is CD8+ T cell-dependent. (A–E) 7 days post treatment initiation, the indicated tissues from CT26-bearing BALB/c mice were examined for the frequency and number of the indicated T cell populations. Data (mean±SD) are pooled from three experiments (n=11/group for TME and spleen; n=6–7/group for TDLN) and analyzed by Mann-Whitney test. (A) CD3+ T cell frequencies, (B) CD8+ T cell frequencies and numbers, (C) CD4+ Tconv and CD4+ Treg frequencies. (D) The numbers of CD8+ T cells and Tregs in the spleen and TDLN. (E) The CD8+ T cell to Treg ratio in the TME, spleen, and TDLN. (F) CT26-bearing mice (n=8–11/group pooled from two experiments) received anti-CD8 to deplete CD8+ T cells 3 days prior (D–3,–2, –1) to administrating HD mIL-2/CD25, represented as D0. Data were analyzed by a log-rank test. HD, high-dose; mIL-2, mouse interleukin-2; PBS, phosphate-buffered saline; TDLN, tumor-draining lymph node; TME, tumor microenvironment; Tregs, regulatory T cells.

unaffected (online supplemental figure 6B). Thus, the increase in neutrophils is not necessary for this antitumor response and may reflect the increased CD8+ tumor-infiltrating lymphocytes (TILs) whose effector response recruits neutrophils to the TME.

HD mIL-2/CD25 enhances the number and function of tumor-antigen specific CD8+ T cells

Given that IL-2R signaling upregulates CD25 on antigen-activated Teff cells, we evaluated CD25 expression on CD8+ T cells in peripheral immune tissues and the TME during HD mIL-2/CD25 therapy. A significant increase in CD25+ CD8+ T cells was noted for the TME, spleen, and TDLN (figure 4A). This finding suggests that in a tumor-burden setting, HD mIL-2/CD25 upregulates CD25 expression on CD8+ tumor-reactive T cells.

To directly investigate the effect of HD mIL-2/CD25 on tumor-reactive T cells, the number of CD8+ T cells specific for AH1 was determined. A time course study revealed a striking increase in percentage and number

of AH1-specific CD8+ T cells in the PBMCs (figure 4B). Although some variability was noted, an increase in AH1+ CD8+ T cells was also detected in the TME and spleen, but not the TDLN (figure 4C) in CT26-bearing mice after treatment with HD mIL-2/CD25.

With respect to functional activity, when CD45-enriched cells from CT26-bearing mice were stimulated ex vivo with the AH1 peptide, HD mIL-2/CD25 supported increased numbers of tumor-specific interferon (IFN)-γ-secreting T cells in the TME, spleen, and TDLN (figure 5A), but with similar mean spot size between phosphate-buffered saline (PBS)-treated and HD mIL-2/CD25-treated mice (online supplemental figure 7), indicative of similar IFN-γ secretion per cell. After re-stimulation in vitro, CD8+ TILs showed an increase in frequency of granzyme B (GrzB)+ cells after stimulation with PMA and ionomycin (figure 5B, top) and trended upward after stimulation with tumor antigen AH1 (figure 5B, bottom). In both settings, these CD8+ TILs produced greater amounts of GrzB, as assessed
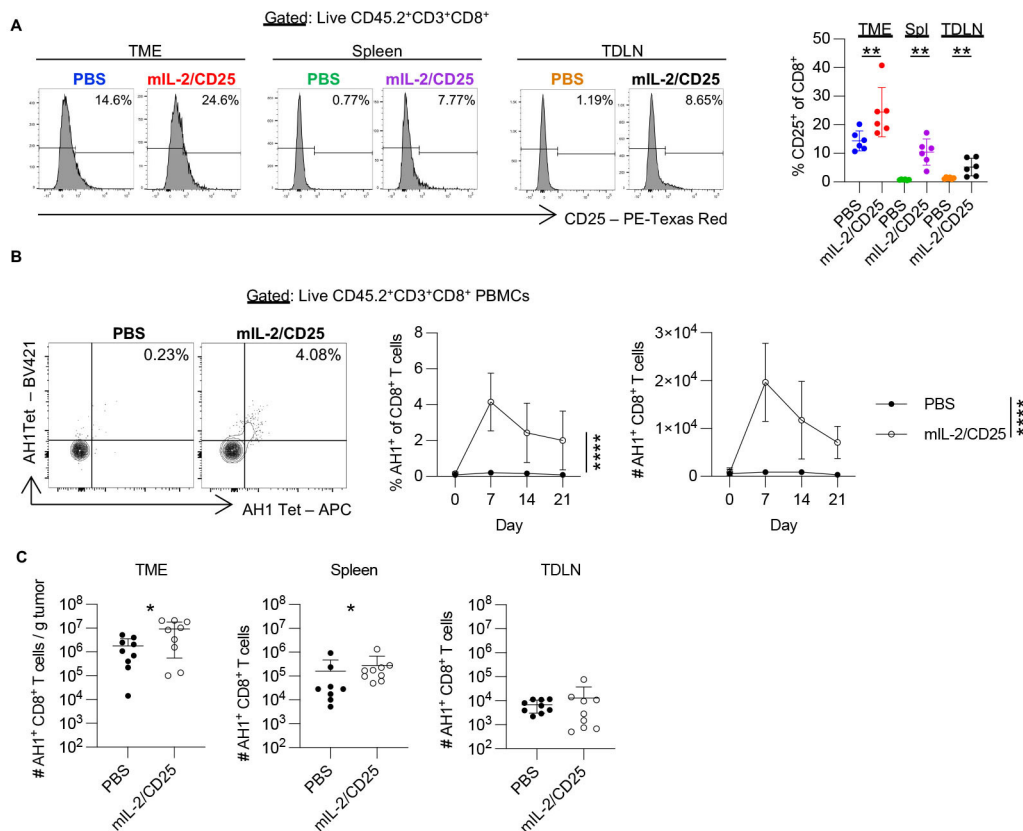
Figure 4 HD mIL-2/CD25 supports increased number of tumor antigen-specific CD8⁺ T cells. (A) 7 days post treatment initiation, the indicated tissues from CT26-bearing mice were examined for CD25 expression by flow cytometry (left, representative flow plot; right, quantitative data). Data (n=6/group pooled from two experiments) are shown as mean±SD and analyzed by Mann-Whitney test. (B) PBMCs from CT26-bearing BALB/c mice were evaluated by flow cytometry for the frequency and number of AH1-specific CD8⁺ T cells during treatment with PBS or mIL-2/CD25. (representative flow plots of D7, left; quantitative data, right). Data (n=5/group pooled from two experiments) are shown as the mean±SD and analyzed by an unpaired t-test with Welch's correction of the area under the curve. (C) 7 days post treatment initiation of CT26-bearing mice, the number of AH1 tetramer-specific CD8⁺ T cells was determined for the indicated tissues. Data (n=9/group pooled from three experiments) are shown as the mean±the SD and analyzed by Mann-Whitney test. HD, high-dose; mIL-2, mouse interleukin-2; PBS, phosphate-buffered saline; PBMCs, peripheral blood mononuclear cells; Spl, spleen; TDLN, tumor-draining lymph node; TME, tumor microenvironment.

by the mean fluorescence intensity (MFI) (figure 5B). In addition, HD mIL-2/CD25 supported a greater percentage of polyfunctional IFNγ⁺ TNF⁺ CD8⁺ TILs after rechallenge in vitro under both conditions (figure 5C). Collectively these data indicate that HD mIL-2/CD25 targets the high-affinity IL-2R on tumor-specific T cells to increase their number and function.

HD mIL-2/CD25 reduces exhaustion of CD8⁺ T cells in the TME

Persistent antigen stimulation that occurs in the TME leads to T cell exhaustion.[28] To test whether HD mIL-2/CD25 might lower T cell exhaustion, the expression of PD-1 and TOX, which are associated with exhausted T cells,[29 30] was examined for CD8⁺ T cells after treatment of CT26-bearing mice with HD mIL-2/CD25 or PBS. In the spleen and TDLN, HD mIL-2/CD25 supported a modest increase in PD-1⁺TOX⁻ CD8⁺ T cells, a finding consistent with an increase in antigen-experienced cells[31] (figure 6A). In contrast, most CD8⁺ TILs expressed PD-1 and TOX (figure 6B). However, HD mIL-2/CD25 supported lower levels of both exhaustion markers, consistent with less

exhausted CD8⁺ T cells (figure 6B,C). In addition, the co-expression of PD-1 with LAG-3, another immune checkpoint associated with exhaustion,[32 33] was selectively lower after HD mIL-2/CD25 treatment (figure 6D).

Expression of TCF1 and PD-1 marks subpopulations of exhausted CD8⁺ T cells, where progenitor-like PD-1⁺TCF1hi CD8⁺ T cells give rise to short-lived terminally exhausted PD-1⁺TCF1lo CD8⁺ T cells.[34–36] A high percentage of progenitor-like PD-1⁺TCF1hi CD8⁺ T cells were found in the TME of PBS-treated and HD mIL-2/CD25-treated mice (figure 6E). However, the number of such cells after HD mIL-2/CD25 were on average 6.5-fold greater, although some variability was noted, and the MFI of PD-1 on these cells was approximately 40% lower (figure 6E). This phenotype in conjunction with lower TOX (figure 6B,C) is consistent with less exhausted CD8⁺ T cells that are expected to be more responsive to checkpoint blockade.[34 37 38] These changes along with lower LAG-3 likely represent effects of HD mIL-2/CD25 on CD8⁺ TILs, although
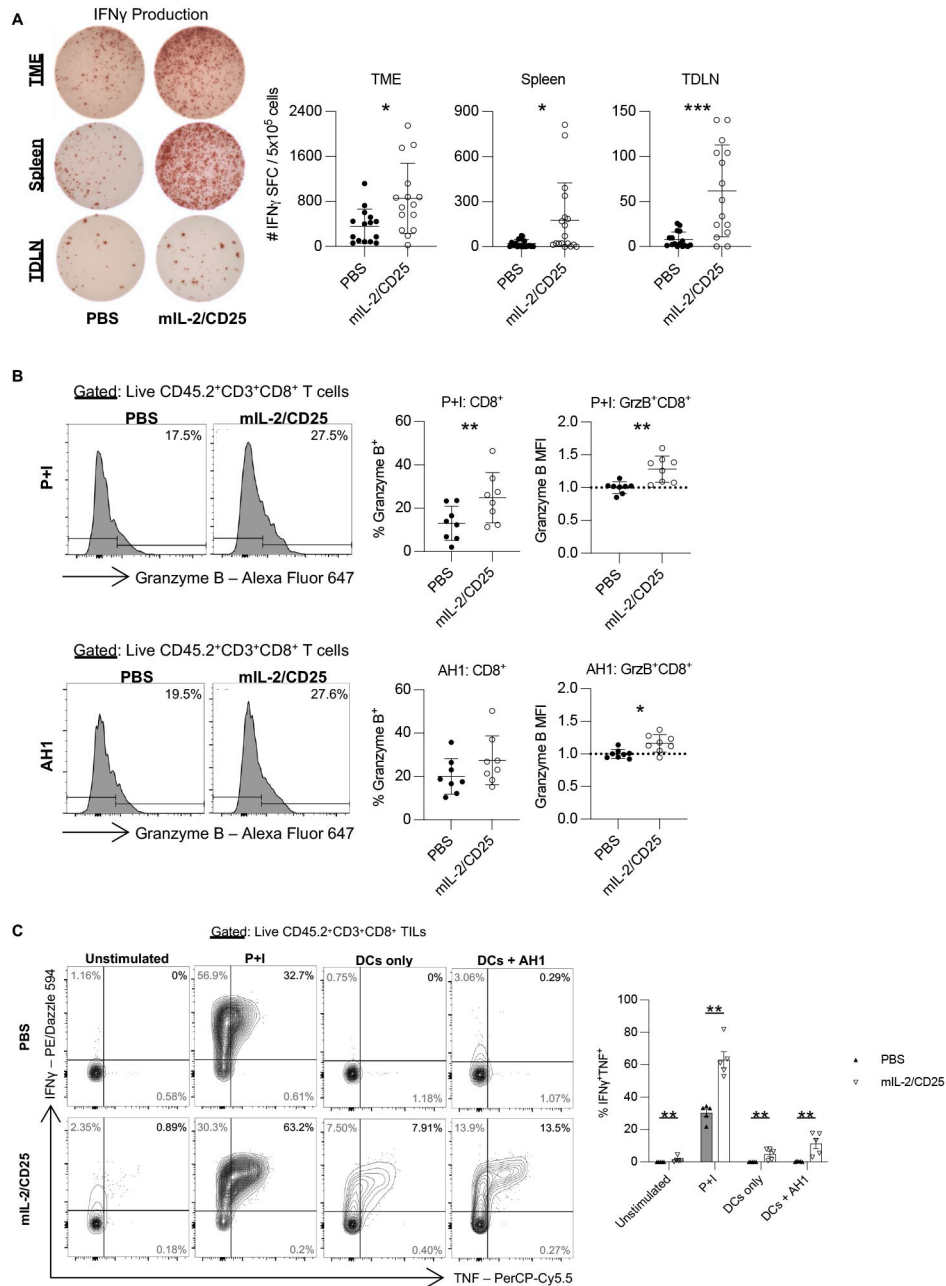
Figure 5 HD mIL-2/CD25 enhances the effector function of tumor antigen-specific CD8^{+} T cells. (A) 7 days post treatment initiation, the indicated tissues from CT26-bearing mice were enriched for CD45^{+} immune cells and examined for IFN-γ-secreting cells by ELISpot (Enzyme-Linked ImmunoSpot) assay (representative wells, left; quantitative data of spot-forming cells (SFC), right) 19–24 hours post in vitro restimulation with BMDCs in the presence or absence of AH1 peptide (2 μg/mL). Data (n=15–18/group pooled from five experiments) are mean±SD and were analyzed by Mann-Whitney test. (B–C) CD45-enriched tumor-associated immune cells were also restimulated in vitro in the presence of PMA and ionomycin (P+I) or BMDCs in the presence (DCs+AH1) or absence (DCs only) of AH1 peptide (10 μg/mL). Cytokine production was evaluated by flow cytometry 4 hours after restimulation. (B) Frequency of and corresponding MFIs of granzyme B-expressing CD8^{+} T cells is shown (representative histograms, left; quantitative data, right). Data (n=8/group pooled from three experiments) are mean±SD and analyzed by Mann-Whitney test. (C) Frequency of IFN-γ^{+} TNF^{+} double cytokine-producing CD8^{+} T cells is shown (representative flow plots, left; quantitative data, right). Data (n=5/group are representative of one experiment) are mean±SD and were analyzed by Mann-Whitney test within each condition. BMDCs, bone marrow-derived DCs; DCs, dendritic cells; GrzB, granzyme B; HD, high-dose; IFN, interferon; MFI, mean fluorescence intensity; mIL-2, mouse interleukin-2; PBS, phosphate-buffered saline; TDLN, tumor-draining lymph node; TILs, tumor-infiltrating lymphocytes; TME, tumor microenvironment.

we cannot rule out that decreased tumor burden will provide lower antigenic stimulation, and this may also contribute to these effects. These phenotypic data in conjunction with the increased number and function of AH1 tumor-specific T cells (figures 4 and 5) and enhanced antitumor responses (figures 1 and 2)
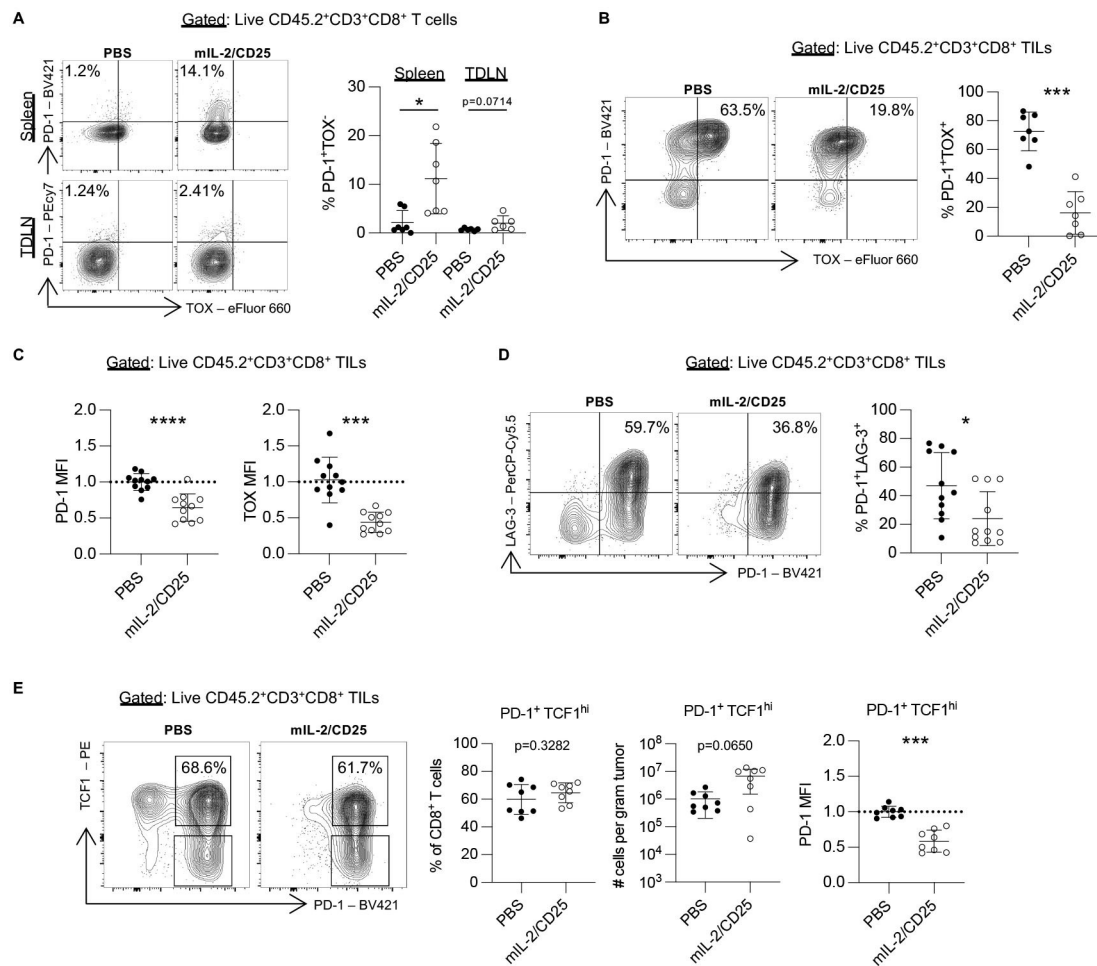
Figure 6 CD8$^+$ T cells from HD mIL-2/CD25-treated CT26-bearing mice are less phenotypically exhausted. (A–D) 7 days post treatment initiation, the indicated tissues from CT26-bearing mice were examined for markers characteristic of CD8$^+$ T cell exhaustion. (A) The frequency of PD-1$^+$TOX$^-$ cells of total CD8$^+$ T cells in the spleen and TDLN is shown in addition to (B) the frequency of PD-1$^+$TOX$^+$ of total CD8$^+$ T cells in the TME (representative flow plots, left; quantitative data, right). Data (n=6–7/ group pooled from two experiments) are mean±SD and analyzed by Mann-Whitney test. (C) The normalized MFI of PD-1 and TOX are shown for CD8$^+$ T cells in the TME. Data (n=11/group pooled from four experiments) are mean±SD and analyzed via Mann-Whitney test. (D) The frequency of PD-1$^+$LAG-3$^+$ of total CD8$^+$ T cells in the TME is shown (representative flow plots, left; quantitative data, right). Data (n=11/group pooled from four experiments) are mean±SD and analyzed by Mann-Whitney test. (E) The frequency, number, and normalized PD-1 MFI of PD-1$^+$ TCF1^{hi} CD8$^+$ T cells in the TME is shown (representative flow plots, left; quantitative data, right). Data (n=8/group, pooled from two experiments) are mean±SD and analyzed via Mann-Whitney test. mIL-2, mouse interleukin-2; MFI, mean fluorescence intensity; PBS, phosphate-buffered saline; TDLN, tumor-draining lymph node; TILs, tumor-infiltrating lymphocytes.

are consistent with a role for targeting CD8$^+$ T cells expressing the high-affinity IL-2R by HD mIL-2/CD25 to promote less exhausted CD8$^+$ T cells with high antitumor activity.

Antitumor immunity by HD-mIL-2/CD25 is enhanced by co-administering anti-PD-1

While the frequency of PD-1$^+$ CD8$^+$ T cells remained high, the relative PD-1 expression on tumor-infiltrating CD8$^+$ T cells was decreased with treatment (figure 6B,C). This is a good prognosis for the therapeutic efficacy of PD-1 blockade[39] and therefore led us to investigate the effects of PD-1 blockade in conjunction with HD mIL-2/CD25 therapy. HD mIL-2/CD25 alone, but not anti-PD-1, supported tumor-free survival in approximately 50% of the mice, as previously observed (figure 1A and figure 7A). However, the combination of HD mIL-2/CD25 plus anti-PD-1 was much more effective, where approximately 90% of the mice were long-term survivors (figure 7A, online supplemental figure 8A). When these latter mice were rechallenged with CT26, all mice remained tumor-free, indicative of the induction of immune memory (figure 7B). In additional cohorts of mice, unlike the synergistic activity between HD mIL-2/CD25 and anti-PD-1, combining anti-PD-1 with S4B6-IL2/IC (figure 7C, online supplemental figure 8B) did not support vigorous antitumor responses. Thus, targeting the high-affinity IL-2R is essential for increasing
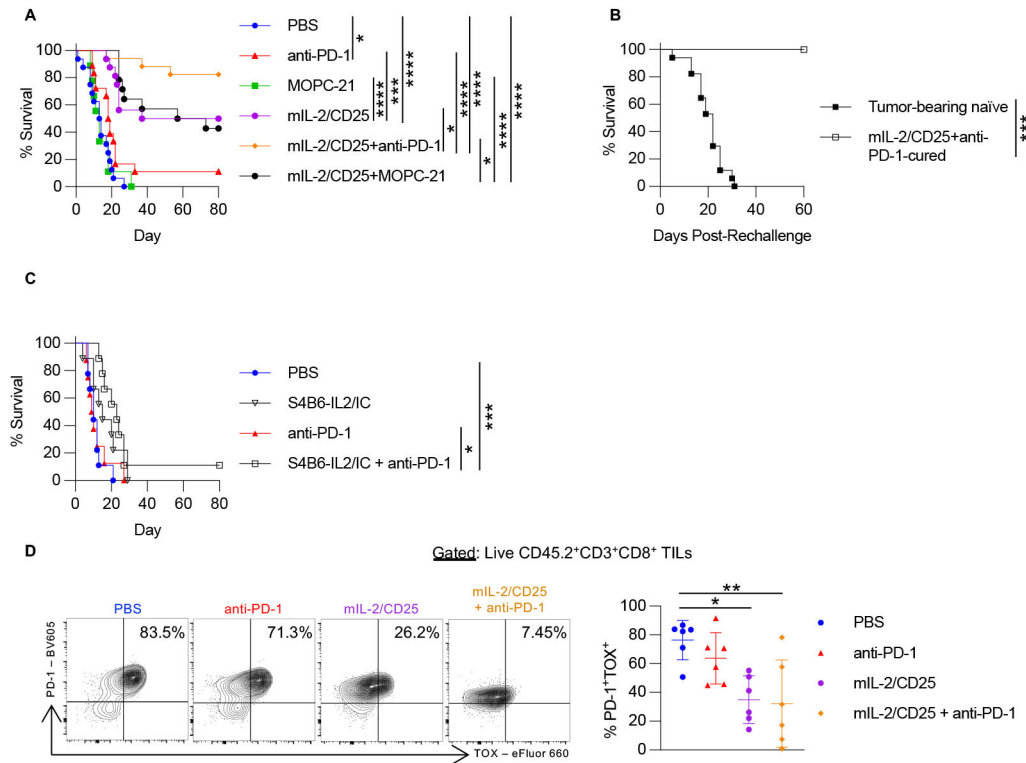
Figure 7 HD mIL-2/CD25 and PD-1 blockade generate highly effective antitumor activity. (A) CT26-bearing mice were treated with PBS, anti-PD-1 (200 µg), MOPC-21 IgG isotype control (200 µg), mIL-2/CD25 (100 µg), or combination therapy as indicated (n=9–18/group pooled from three experiments) and survival was determined. Data were analyzed by a log-rank test. (B) Naïve mice or mice that cleared CT26 after combination therapy (mIL-2/CD25+anti-PD-1) were rechallenged with CT26 90 days after primary tumor clearance and survival was determined. Data (n=4/group pooled from two experiments) were analyzed by a log-rank test. (C) CT26-bearing mice were treated with PBS, anti-PD-1 (200 µg), S4B6-IL2/IC (1.5 µg mIL-2/15 µg S4B6), or combination therapy as indicated and survival was determined. Data (n=8–9/group pooled from two experiments) were analyzed by a log-rank test. (D) 7 days post treatment initiation in the experiments described in A, TILs from CT26-bearing mice were examined for expression of PD-1 and TOX (representative flow plots, left; quantitative data, right). Data (n=6/group pooled from two experiments) are mean±SD and analyzed by one-way analysis of variance with Tukey's multiple comparison test. HD, high-dose; IC, immune-complexes; mIL-2, mouse interleukin-2; PBS, phosphate-buffered saline; TILs, tumor-infiltrating lymphocytes.

antitumor immunity when applied with anti-PD-1 checkpoint blockade.

When TILs from CT26-bearing mice were examined during the primary antitumor response, mIL-2/CD25 supported a reduction of PD-1+TOX+ CD8+ T cells and this effect was at best only slightly increased when HD mIL-2/CD25 was combined with anti-PD-1 (figure 7D). Thus, preferential IL-2R signaling through the high-affinity IL-2R is the main driver of CD8+ T cells with a less exhausted phenotype in this combination therapy.

DISCUSSION

Our study demonstrates that stimulating the high-affinity IL-2R on tumor-specific CD8+ Teff cells is essential for effective IL-2-dependent antitumor immunotherapy. HD mIL-2/CD25 monotherapy, which targets the high-affinity IL-2R, supported substantial antitumor responses against highly immunogenic tumors and when combined with anti-PD-1 checkpoint blockade, tumors were eradicated in essentially all mice. These findings contrast with the consensus that targeting the intermediate-affinity IL-2R is the best strategy for IL-2-dependent antitumor

immunotherapy due to its ability to limit undesired activation of Tregs. However, even though HD mIL-2/CD25 increases Tregs, it supported more robust antitumor responses than using an IL2/IC that targets the intermediate-affinity IL-2R. The IL2/ICs were used at a dose and administered in a manner that preferentially expanded MP CD8+ T and NK cells over Tregs and generated antitumor immune responses similar to that reported by other studies.[18–24] Our findings highlight that a limitation of broadly increasing CD8+ T cells, even with an accompanying expansion of NK cells, is an insufficient increase of tumor antigen-specific CD8+ T cells, which are the critical cells for effective antitumor immunity.

The half-lives and modes of action of mIL-2/CD25 and S4B6-IL2/IC are different,[6 12 21 22] complicating the experimental design comparing these two agents. We used an amount of S4B6-IL2/IC that has been commonly used in other studies[18–24] exploring antitumor activity by targeting the intermediate affinity IL-2R. The frequency of administration of S4B6-IL2/IC has been somewhat more variable as in some studies it was administered daily for 3–5 days whereas other studies administered the IL2/

9

IC every other day. Based on this concern, we confirmed that 1.5 µg of IL-2 associated with 15 µg S4B6 yielded high expansion of CD8^{+} T and NK cells while minimally affecting Tregs when administered as a single injection or when treating tumor-bearing mice with a therapeutic regimen. We found selective expansion of CD8^{+} T and NK cells by our regimen not only after a single administration of S4B6-IL2/IC, but also during therapeutic dosing. We cannot rule out improved anticancer responses if we administered greater amounts of S4B6-IL2/IC. However, we believe we are approaching the maximal dosing and frequency of S4B6-IL2/IC because when we modestly increased the dose of S4B6-IL2/IC to 5 µg IL-2/50 µg S4B6, severe toxicity resulted, likely from a cytokine storm due to high expansion of CD8^{+} and NK cells. 100 µg of mIL-2/CD25 is a much larger dose of IL-2 than 1.5 µg IL-2/15 µg S4B6. However, this fusion protein is administered largely as an inactive dimer, where we have previously estimated that only a small fraction, approximately 1%, at any time is biologically active as mIL-2/CD25 monomers slowly and continually dissociate from the inactive dimer.[12] Thus, administration of 100 µg of mIL-2/CD25 results in roughly 1 µg of active mIL-2/CD25 monomers that are continually released over several days from the dimers, which approximates the dose of S4B6-IL2/IC used to treat the tumor-bearing mice.

In addition, many studies targeting the intermediate affinity IL-2R using S4B6-IL2/IC[18–24] or other modified IL-2s[40] have shown antitumor effects and some of these were more robust than we observed. An important difference in our study with most previous reports is that we initiated IL-2-dependent immunotherapy much later in tumor progression. Thus, it is unlikely that our antitumor responses using S4B6-IL2/IC represent a limitation due to its dose and frequency. Importantly, our experimental design demonstrates the high activity of HD mIL-2/CD25 in supporting antitumor responses to immunogenic tumors.

Recombinant IL-2 therapy is highly effective in a small fraction of patients with melanoma or renal cell carcinoma,[2 41] two tumors that are considered immunogenic.[42] Immunosuppression of the antitumor response by off-target Tregs is considered one of the underlying factors for the low response rate.[43 44] Although this is a potential contributing factor, our study raises two other possibilities. Effective antitumor responses by HD mIL-2/CD25 required a sufficient number of pre-existing tumor-specific T cells, as this approach worked best with highly immunogenic MC38 and CT26 tumors. Thus, patients with low numbers of pre-existing tumor-specific T cells are unlikely to respond to recombinant IL-2 immunotherapy. In this case, vaccination with neoantigen vaccines might increase the frequency of pre-existing tumor-reactive T cells to be targeted by IL-2-based therapies.[14 15] Moreover, the high amount of recombinant IL-2 that is infused into patients with cancer stimulates both cells that express the high-affinity and the intermediate-affinity IL-2R. Thus, the broad expansion of MP CD8^{+} T and NK cells may have limited the effectiveness to expand the low frequency of tumor antigen-specific T cells that express the high-affinity IL-2R. These latter two issues do not come into play with HD mIL-2/CD25 even though the active moiety is wild-type IL-2. mIL-2/CD25 has properties analogous to an IL-2 mutein with preferential reactivity toward the high-affinity IL-2R, as the majority of the administered material is in a transdimer configuration, where all IL-2 activity is masked. The slow dissociation of dimer into the active monomer at the amounts used did not reach concentrations high enough to cause the expansion of MP CD8^{+} and NK cells that only express the intermediate-affinity IL-2R.

Our data indicate that HD mIL-2/CD25 on its own leads to the expansion of a population of less exhausted CD8^{+} T cells within the TME. Similar results have recently been reported, where IL-2 and anti-PD-L1 act in concert to promote immunity to chronic LCMV infection[45 46] and to orthotopically implanted Panc02-H7-Fluc pancreatic adenocarcinoma.[47] Both studies showed that IL-2R signaling promoted the development of highly functional CD8^{+} Teff cells from PD-1^{+} TCF1^{hi} stem-like cells, which are precursors to terminally exhausted cells. However, neither study addressed the efficacy of preferentially targeting the high-affinity IL-2R for antitumor immunity. When only recombinant IL-2 was used, an effective antiviral response did not occur; a reduction in viral titers required co-administration of anti-PD-L1.[45 46] Potent immunity was observed with an engineered IL-2/anti-PD-1 fusion protein biased to IL-2Rβ and γc that targeted the IL-2 activity toward viral-specific and tumor-antigen-specific CD8^{+} T cells, but not most Tregs.[47] Our study extends these findings by showing that stimulation of the high-affinity IL-2R with mIL-2/CD25 on tumor-specific CD8^{+} T cells is required for optimal antitumor responses, even though substantial increases in Tregs occurred. The antitumor responses occurred in part because the TME contained a high ratio of CD8^{+} T cells to Tregs. Our study indicates that increases in Tregs during antitumor responses are not limiting when coupled to sufficient expansion of tumor-reactive T cells using mIL-2/CD25 alone or with anti-PD-1. Improving the efficiency of checkpoint blockade for tumor immunotherapy is under intense investigation. Combination of HD mIL-2/CD25 with anti-PD-1 may enable very effective improvement of the tumor-specific CD8^{+} T cell response coupled with expansion of Tregs outside the TME to limit the many autoimmune-like side effects that accompany checkpoint blockade.[48 49]

METHODS

Mice

BALB/cJ (JAX stock #000651) and C57Bl/6J (JAX stock #000664) mice were purchased from The Jackson Laboratory. Female mice, 6–9 weeks old, were used in all experiments shown. When male mice were included (not shown), no obvious sex differences were observed

in therapeutic responses. Mice were housed in a specific pathogen-free facility. Animal studies were approved by the Institutional Animal Care and Use Committee at the University of Miami (Protocols 18–147, 21–151).

IL-2-based biologics

The mIL-2/CD25 was purified from culture supernatants of mIL-2/CD25-transfected Chinese Hamster Ovary (CHO) cells as previously described.[12] Mouse IL-2 (mIL-2) (Peprotech, cat. #212–12) was reconstituted based on manufacturer's recommendations: reconstituted at 0.5 mg/mL in H_2O containing 0.1% bovine serum albumin (BSA) and stocks were stored at –80°C. Anti-mIL-2 clone S4B6-1 (S4B6) (Bio X Cell, InVivoMAb, cat #BE0043-1) was stored at 4°C. Immune-complexes were formed by mixing mIL-2 and S4B6 at the indicated amounts at a 2:1 molar ratio in PBS and incubating at 37°C for 30 min before intraperitoneal (i.p.) injection, as previously described.[6]

In vivo tumor models

CT26 colon carcinoma, MC38 colon adenocarcinoma, B16.F10 melanoma, and 4T1 mammary carcinoma cells were purchased from American Type Culture Collection, tested and verified to be negative for mycoplasma and other pathogenic agents. CT26, B16.F10, and 4T1 were cultured in RPMI-1640 media supplemented with 5% fetal bovine serum (FBS), 100 U/mL penicillin, 100 μg/mL streptomycin, 2 mM L-glutamine, 0.05 mM β-mercaptoethanol, and 1 mM sodium pyruvate (RPMI 1640 complete media or RPMI-CM). MC38 was cultured in DMEM (Dulbecco's Modified Eagle's Medium) supplemented with 5% FBS, 100 U/mL penicillin, 100 μg/mL streptomycin, 2 mM L-glutamine, 0.05 mM β-mercaptoethanol, and 1 mM sodium pyruvate. Tumor cells were incubated at 37°C in a humified incubator at 5% CO_2. On initial thawing, the tumor cells were expanded, and aliquots were frozen to allow use of low passage cells throughout the study. The thawed cells were maintained in culture for less than 2 weeks. CT26 (1×10^6) were inoculated subcutaneously into the rear flank of BALB/cJ mice. MC38 (5×10^5) and B16.F10 (1×10^5) were inoculated subcutaneously into the rear flank of C57Bl/6 mice. 4T1 (1×10^5) were inoculated orthotopically in the mammary fat pad of BALB/cJ mice. In rechallenge studies, BALB/cJ mice were inoculated with CT26 (1×10^6). Tumor growth was monitored by measuring two opposing diameters with standard calipers. Results are presented as tumor volume (mm^3), where volume was calculated using the formula: $((L \times W^2)/2)$ where L=length, W=width and L≥W. Therapy was initiated once average tumor size was approximately 100–200 mm^3 (CT26: 12–14 days, MC38: 9–10 days, B16.F10: 6–7 days, and 4T1: 9–10 days post-inoculation). All mice were randomized based on tumor volume prior to the start of therapy (D0). In survival studies, mice were sacrificed when tumor volume reached ≥2000 mm^3 or L≥15 mm.

Preparation of PBMCs and secondary lymphoid tissues

PBMCs were collected from mice via submandibular bleeding using an 18G needle and mixed with 3 μl heparin (5 units/μl) to prevent coagulation. 50 μl blood from each sample was washed 1× with Hanks's balanced salt solution (HBSS). After careful removal of supernatant, red blood cells were lysed from PBMCs using ACK lysis buffer (0.2% Tris pH 7.6 and 0.75% ammonium chloride) by incubating the blood with 2 mL ACK lysis buffer for 5 min in a 37°C water bath. Cells were then washed 1× with HBSS and then resuspended in FACS buffer (HBSS containing 0.2% BSA and 0.1% w/v sodium azide) for flow cytometry staining. Spleens and TDLNs (inguinal lymph nodes taken only from the side of the tumor) were harvested and single cell suspensions produced via mechanical disruption. Splenocytes were incubated with an ACK lysis buffer for 1 min in a 37°C water bath, and washed 1× with HBSS. Cell pellets from spleen and TDLN were resuspended in RPMI-CM, passed through a 70 μm filter, and counted. Cells were then resuspended in FACS buffer for flow cytometry staining or kept in RPMI-CM for functional assays.

Preparation of tumor-infiltrating lymphocytes

For CT26 TME studies, on day 7 of therapy, tumors were excised, weighed, and minced into 1–2 mm pieces. Tumors were incubated at 37°C with gentle shaking in RPMI-CM containing 1 mg/mL Collagenase from Clostridium histolyticum (Sigma cat. #C5138) for 20 min. Single cell suspensions were then obtained using gentleMACS C Tubes (Miltenyi Biotec, cat. #130096334) and the gentleMACS Dissociator. Single cell suspensions were washed 1× with RPMI-CM to remove Collagenase. Cell pellets were resuspended with 2 mL ACK lysis buffer for 3 min in a 37°C water bath, then washed 1× with HBSS. Cell pellets were resuspended in 10 mL RPMI-CM, passed through a 70 μm filter, counted, and prepared for CD45 enrichment and/or stained for flow cytometry. Mouse CD45 microbeads (Miltenyi Biotec, cat. #130-052-301), LS columns (Miltenyi Biotec, cat. #130-042-401), and a quadroMACS Separator (Miltenyi Biotec, cat. #130-091-051) were used per manufacturer's recommendations to isolate CD45-expressing immune cells from the CT26 TME for functional assays.

Flow cytometric analysis

Antibodies used for flow cytometry are shown in online supplemental table 1. Cells in the FACS buffer were incubated with 2.4G2 for 1 min to block Fc receptors. After washing 1× with FACS buffer, cells were incubated with antibodies for extracellular staining for 15 min at 4°C and then washed 1× with FACS buffer. For extracellular staining containing fixable viability dye, this staining was performed in and washed with HBSS instead of FACS buffer for optimal live/dead staining. Intracellular staining was performed following permeabilization and fixation using the eBioscience Foxp3 Transcription Factor Staining Buffer Set (Thermo Fisher, Invitrogen,

cat. #00-5523-00) using the manufacturer's instructions. For quantification of populations in PBMC samples, exactly 50 µL of blood was stained and the entire sample was run on the flow cytometer. Samples were run on BD LSR-Fortessa-HTS or Beckman Coulter CytoFLEX LX and data were analyzed using FlowJo (V.10.8) software.

Tetramer staining
Cells in the FACS buffer were incubated with 2.4G2 for 5 min at room temperature. Cells were washed 1× with FACS buffer and on resuspension, incubated with APC-labeled and/or BV421-labeled tetramer(s) to AH1 (SPSYVYHQF, class I MHC H-2L^d) and anti-CD8-FITC for 1 hour in the dark at room temperature. Additional extracellular/viability and intracellular staining was performed as described above.

Depletion and blocking antibodies
For CD8$^+$ T cell depletion, anti-CD8β Lyt 3.2 clone 53–5.8 (Bio X Cell, InVivoMAb, cat. #BE0223) was i.p. injected at 100 µg per mouse on D −3, −2, and −1, where IL-2-targeted and PD-1-targeted therapies started on D0. For neutrophil depletion, anti-Ly6G clone 1A8 (Bio X Cell, InVivoMAb, cat. #BE0075-1) was i.p. injected at 150 µg per mouse on D−1, 1, 3, 5, 7, 9, and 11. For PD-1 blockade, anti-mPD1-4H2-mg1-D265A (mouse IgG1 antibody clone 4H2 with a D265A point mutation to prevent binding to Fc receptors, provided by Bristol Myers Squibb) was i.p. injected at 200 µg per mouse and co-administered with mIL-2/CD25 (D0, 3.5, 7, 10.5, and 14). MOPC-21, an IgG1 isotype control of unknown specificity (Bio X Cell, InVivoMAb, cat #BE0083), was i.p. injected at 200 µg per mouse in parallel with anti-PD-1.

Generation of bone marrow-derived dendritic cells
Femur bones were collected from BALB/cJ mice, muscle tissue removed, and bones sterilized in a petri dish containing 70% ethanol for 1 min. The bones were then washed by two consecutive immersions in petri dishes containing 1× PBS for 1 min each. Bones were then crushed in cold 1× HBSS via a pestle and collected by centrifugation (1200 rpm, 5 min, 4°C). Cell pellets were resuspended in 2 mL ACK lysing buffer lysing buffer, incubated for 2 min, and washed with HBSS. The cell pellets were resuspended in 5 mL of RPMI-CM and filtered through a 70 µm cell strainer. Bone marrow cells ($10×10^6$) were cultured in 10 mL RPMI-CM containing 20 ng/mL recombinant mouse GM-CSF (rmGM-CSF, PeproTech, Cat. No. 315–03) using 100×15 mm culture dishes (VWR, Cat. No. 25 384–342) at 37°C in a humidified atmosphere at 5% CO_2. On day 3, an additional 10 mL of RPM1-CM containing 20 ng/mL rmGM-CSF was added to each plate. On days 6 and 8, 10 mL (50%) of the media was removed from each plate and any non-adherent cells were collected by centrifugation. These cell pellets were resuspended in 10 mL RPMI-CM containing 20 ng/mL rmGM-CSF and added back to the corresponding culture dish. To mature the DCs, on day 10, non-adherent cells

from each culture plate were harvested, cells were centrifuged, and the cell pellets were resuspended in 10 mL RPMI-CM containing 10 ng/mL rmGM-CSF and 1 µg/mL LPS (lipopolysaccharides from *Escherichia coli* O55:B5, Millipore Sigma, cat. No. L2880) and re-plated in a new 100×15 mm culture dish. On day 11, 10 mL RPMI-CM was added to each dish. On day 12, adherent bone marrow-derived DCs (BMDCs) were collected using a cell scraper, frozen in 90% FBS and 10% dimethyl sulfoxide (DMSO), and stored at −150°C until used in vitro.

Enzyme-Linked ImmunoSpot assay
ELISpot assays were performed following manufacturer's protocols using the Mouse IFN-γ Enzyme-Linked ImmunoSpot (ELISpot) set (BD Biosciences Cat. No. 551083). In brief, serial dilutions of lymphoid cells from the spleen, draining lymph node, or TILs were cultured in RPMI-CM with or without AH1 tumor antigen peptide (2 µg/mL; ChiScientific, sequence: SPSYVYHQF) and 10-fold lower numbers of BMDCs in anti-IFN-γ-coated (5 µg/mL antibody incubation overnight, BD Biosciences Cat. No. 551881) 96-well ELISpot plates (Millipore Sigma Cat. No. S2EM004M99) for 19–24 hours at 37°C in 5% CO_2. Secretion of IFN-γ was detected using biotinylated anti-IFN-γ (2 µg/mL, BD Biosciences Cat. No. 551881) followed by the addition of Streptavidin-HRP (1:100, BD Biosciences Cat. No. 557630) and AEC Chromogen/Substrate (BD Biosciences, Cat. No. 551951). ELISpots were visualized using ImmunoSpot S6 Universal and quantified using ImmunoSpot V.7.0.30.4 Analyzer Professional DC software.

Intracellular cytokine assay
Single cell suspensions from spleen, TDLN, and TME ($2.5×10^5$/well) with BMDCs ($2.5×10^4$/well) were incubated in 48-well plates in RPMI-CM, AH1 peptide (10 µg/mL), Monensin (1:1000, BD GolgiStop Protein Transport Inhibitor, BD Biosciences, Cat. No. 51-2092KZ), and Brefeldin A (1:1000, BioLegend Brefeldin A Solution, Cat. No. 420601) for 4 hours at 37°C in 5% CO_2. Cells were harvested and prepared for flow cytometric analysis as described above, except intracellular cytokine staining was performed following permeabilization and fixation using the BD CytoFix/CytoPerm Solution Kit (BD Biosciences, cat. No. 554714) using the manufacturer's instructions.

Statistical analysis
All data are expressed as mean±SD. Statistical analyses were performed using GraphPad Prism V.9 software. For two-group analyses, Mann-Whitney test was used. For three or more groups, one-way analysis of variance (ANOVA) with Tukey's multiple comparison test was used. Blood data containing multiple time points was analyzed by Kruskal-Wallis multiple comparison test of each time point or area under the curve (AUC) analysis. For two-group analyses of AUC, a Welch's t-test was performed. For three or more group analyses of AUC, a one-way ANOVA with

Tukey's multiple comparison test was performed. Survival data are expressed using the Kaplan-Meier method and analyzed via log-rank (Mantel-Cox) test. All tests are listed in the corresponding figure legends. Significance is indicated by * = p<0.05, ** = p<0.01, *** = p<0.001, and **** = p<0.0001.

ORCID iD
Thomas R Malek http://orcid.org/0000-0001-7174-0434

REFERENCES

1. Fyfe GA, Fisher RI, Rosenberg SA, *et al*. Long-term response data for 255 patients with metastatic renal cell carcinoma treated with high-dose Recombinant Interleukin-2 therapy. *J Clin Oncol* 1996;14:2410–1.
2. Atkins MB, Lotze MT, Dutcher JP, *et al*. High-dose Recombinant interleukin 2 therapy for patients with metastatic Melanoma: analysis of 270 patients treated between 1985 and 1993. *J Clin Oncol* 1999;17:2105–16.
3. Overwijk WW, Tagliaferri MA, Zalevsky J. Engineering IL-2 to give new life to T cell Immunotherapy. *Annu Rev Med* 2021;72:281–311.
4. Hernandez R, Põder J, LaPorte KM, *et al*. Engineering IL-2 for Immunotherapy of autoimmunity and cancer. *Nat Rev Immunol* 2022;22:614–28.
5. Baluna R, Vitetta ES. Vascular leak syndrome: a side effect of Immunotherapy. *Immunopharmacology* 1997;37:117–32.
6. Boyman O, Kovar M, Rubinstein MP, *et al*. Selective stimulation of T cell Subsets with antibody-cytokine immune complexes. *Science* 2006;311:1924–7.
7. Tang Q, Adams JY, Penaranda C, *et al*. Central role of defective Interleukin-2 production in the triggering of Islet autoimmune destruction. *Immunity* 2008;28:687–97.
8. Spangler JB, Tomala J, Luca VC, *et al*. Antibodies to Interleukin-2 elicit selective T cell subset potentiation through distinct conformational mechanisms. *Immunity* 2015;42:815–25.
9. Yuan X, Dong Y, Tsurushita N, *et al*. Cd122 blockade restores immunological tolerance in autoimmune type 1 diabetes via multiple mechanisms. *JCI Insight* 2018;3.
10. Church SE, Jensen SM, Antony PA, *et al*. Tumor-specific Cd4^{+} T cells maintain Effector and memory tumor-specific Cd8+ T cells. *Eur J Immunol* 2014;44:69–79.
11. Tay RE, Richardson EK, Toh HC. Revisiting the role of Cd4^{+} T cells in cancer Immunotherapy-new insights into old paradigms. *Cancer Gene Ther* 2021;28:5–17.
12. Ward NC, Yu A, Moro A, *et al*. IL-2/Cd25: A long-acting fusion protein that promotes immune tolerance by selectively targeting the IL-2 receptor on regulatory T cells. *J Immunol* 2018;201:2579–92.
13. Ward NC, Lui JB, Hernandez R, *et al*. Persistent IL-2 receptor signaling by IL-2/Cd25 fusion protein controls diabetes in NOD mice by multiple mechanisms. *Diabetes* 2020;69:2400–13.
14. Hernandez R, Toomer KH, Põder J, *et al*. Sustained IL-2R signaling of limited duration by high-dose mIL-2/Mcd25 fusion protein Amplifies tumor-reactive Cd8^{+} T cells to enhance antitumor immunity. *Cancer Immunol Immunother* 2021;70:909–21.
15. Hernandez R, LaPorte KM, Hsiung S, *et al*. High-dose IL-2/Cd25 fusion protein Amplifies vaccine-induced Cd4+ and Cd8+ Neoantigen-specific T cells to promote antitumor immunity. *J Immunother Cancer* 2021;9:e002865.
16. Huang AY, Gulden PH, Woods AS, *et al*. The Immunodominant major Histocompatibility complex class I-restricted antigen of a murine colon tumor derives from an endogenous retroviral Gene product. *Proc Natl Acad Sci U S A* 1996;93:9730–5.
17. McMahan RH, McWilliams JA, Jordan KR, *et al*. Relating TCR-peptide-MHC affinity to Immunogenicity for the design of tumor vaccines. *J Clin Invest* 2006;116:2543–51.
18. Kamimura D, Sawa Y, Sato M, *et al*. IL-2 in vivo activities and antitumor efficacy enhanced by an anti-IL-2 mAb. *J Immunol* 2006;177:306–14.
19. Jin G-H, Hirano T, Murakami M. Combination treatment with IL-2 and anti-IL-2 mAbs reduces tumor metastasis via NK cell activation. *Int Immunol* 2008;20:783–9.
20. Verdeil G, Marquardt K, Surh CD, *et al*. Adjuvants targeting innate and adaptive immunity Synergize to enhance tumor Immunotherapy. *Proc Natl Acad Sci U S A* 2008;105:16683–8.
21. Tomala J, Chmelova H, Mrkvan T, *et al*. In vivo expansion of activated naive Cd8+ T cells and NK cells driven by complexes of IL-2 and anti-IL-2 Monoclonal antibody as novel approach of cancer Immunotherapy. *J Immunol* 2009;183:4904–12.
22. Létourneau S, van Leeuwen EMM, Krieg C, *et al*. IL-2/anti-IL-2 antibody complexes show strong biological activity by avoiding interaction with IL-2 receptor A subunit Cd25. *Proc Natl Acad Sci USA* 2010;107:2171–6.
23. Krieg C, Létourneau S, Pantaleo G, *et al*. Improved IL-2 Immunotherapy by selective stimulation of IL-2 receptors on lymphocytes and endothelial cells. *Proc Natl Acad Sci USA* 2010;107:11906–11.
24. Tomala J, Chmelova H, Strohalm J, *et al*. Antitumor activity of IL-2/anti-IL-2 mAb Immunocomplexes exerts synergism with that of N-(2-Hydroxypropyl)Methacrylamide Copolymer-bound doxorubicin conjugate due to its low immunosuppressive activity. *Int J Cancer* 2011;129:2002–12.
25. Tomala J, Weberova P, Tomalova B, *et al*. IL-2/Jes6-1 mAb complexes dramatically increase sensitivity to LPS through IFN-Γ production by Cd25^{+}Foxp3^{-} T cells. *ELife* 2021;10:e62432.
26. Raeber ME, Rosalia RA, Schmid D, *et al*. Interleukin-2 signals converge in a Lymphoid–Dendritic cell pathway that promotes anticancer immunity. *Sci Transl Med* 2020;12:eaba5464.
27. Daley JM, Thomay AA, Connolly MD, *et al*. Use of Ly6G-specific Monoclonal antibody to deplete neutrophils in mice. *J Leukoc Biol* 2008;83:64–70.
28. Wherry EJ. T cell exhaustion. *Nat Immunol* 2011;12:492–9.
29. Wherry EJ, Ha S-J, Kaech SM, *et al*. Molecular signature of Cd8^{+} T cell exhaustion during chronic viral infection. *Immunity* 2007;27:670–84.

30 Khan O, Giles JR, McDonald S, *et al*. TOX Transcriptionally and Epigenetically programs Cd8+ T cell exhaustion. *Nature* 2019;571:211–8.

31 Gros A, Robbins PF, Yao X, *et al*. PD-1 identifies the patient-specific Cd8+ tumor-reactive repertoire infiltrating human tumors. *J Clin Invest* 2014;124:2246–59.

32 Grosso JF, Goldberg MV, Getnet D, *et al*. Functionally distinct LAG-3 and PD-1 Subsets on activated and chronically stimulated Cd8 T cells. *J Immunol* 2009;182:6659–69.

33 Matsuzaki J, Gnjatic S, Mhawech-Fauceglia P, *et al*. Tumor-infiltrating NY-ESO-1-specific Cd8+ T cells are negatively regulated by LAG-3 and PD-1 in human ovarian cancer. *Proc Natl Acad Sci U S A* 2010;107:7875–80.

34 Utzschneider DT, Charmoy M, Chennupati V, *et al*. T cell factor 1-expressing memory-like Cd8(+) T cells sustain the immune response to chronic viral infections. *Immunity* 2016;45:415–27.

35 Wu T, Ji Y, Moseman EA, *et al*. The Tcf1-Bcl6 axis Counteracts type I interferon to repress exhaustion and maintain T cell Stemness. *Sci Immunol* 2016;1.

36 Chen Z, Ji Z, Ngiow SF, *et al*. TCF-1-centered transcriptional network drives an Effector versus exhausted Cd8 T cell-fate decision. *Immunity* 2019;51:840–55.

37 Blackburn SD, Shin H, Freeman GJ, *et al*. Selective expansion of a subset of exhausted Cd8 T cells by ᴀPD-L1 blockade. *Proc Natl Acad Sci U S A* 2008;105:15016–21.

38 Im SJ, Hashimoto M, Gerner MY, *et al*. Defining Cd8+ T cells that provide the proliferative burst after PD-1 therapy. *Nature* 2016;537:417–21.

39 Ngiow SF, Young A, Jacquelot N, *et al*. A threshold level of Intratumor Cd8+ T-cell Pd1 expression dictates therapeutic response to anti-Pd1. *Cancer Res* 2015;75:3800–11.

40 Sahin D, Arenas-Ramirez N, Rath M, *et al*. An IL-2-Grafted antibody Immunotherapy with potent efficacy against metastatic cancer. *Nat Commun* 2020;11:6440.

41 Rosenberg SA. Interleukin 2 for patients with renal cancer. *Nat Clin Pract Oncol* 2007;4:497.

42 Fridman WH, Pagès F, Sautès-Fridman C, *et al*. The immune contexture in human tumours: impact on clinical outcome. *Nat Rev Cancer* 2012;12:298–306.

43 Ahmadzadeh M, Rosenberg SA. IL-2 administration increases Cd4+Cd25Hi Foxp3+ regulatory T cells in cancer patients. *Blood* 2006;107:2409–14.

44 Sim GC, Martin-Orozco N, Jin L, *et al*. IL-2 therapy promotes suppressive ICOS+ Treg expansion in Melanoma patients. *J Clin Invest* 2014;124:99–110.

45 West EE, Jin H-T, Rasheed A-U, *et al*. PD-L1 blockade Synergizes with IL-2 therapy in Reinvigorating exhausted T cells. *J Clin Invest* 2013;123:2604–15.

46 Hashimoto M, Araki K, Cardenas MA, *et al*. PD-1 combination therapy with IL-2 modifies Cd8+ T cell exhaustion program. *Nature* 2022;610:173–81.

47 Codarri Deak L, Nicolini V, Hashimoto M, *et al*. PD-1-cis IL-2R Agonism yields better Effectors from stem-like Cd8+ T cells. *Nature* 2022;610:161–72.

48 Alissafi T, Hatzioannou A, Legaki AI, *et al*. Balancing cancer Immunotherapy and immune-related adverse events: the emerging role of regulatory T cells. *J Autoimmun* 2019;104:102310.

49 Kumar P, Saini S, Prabhakar BS. Cancer Immunotherapy with check point inhibitor can cause autoimmune adverse events due to loss of Treg homeostasis. *Semin Cancer Biol* 2020;64:29–35.

Supplemental material

BMJ Publishing Group Limited (BMJ) disclaims all liability and responsibility arising from any reliance placed on this supplemental material which has been supplied by the author(s)

J Immunother Cancer
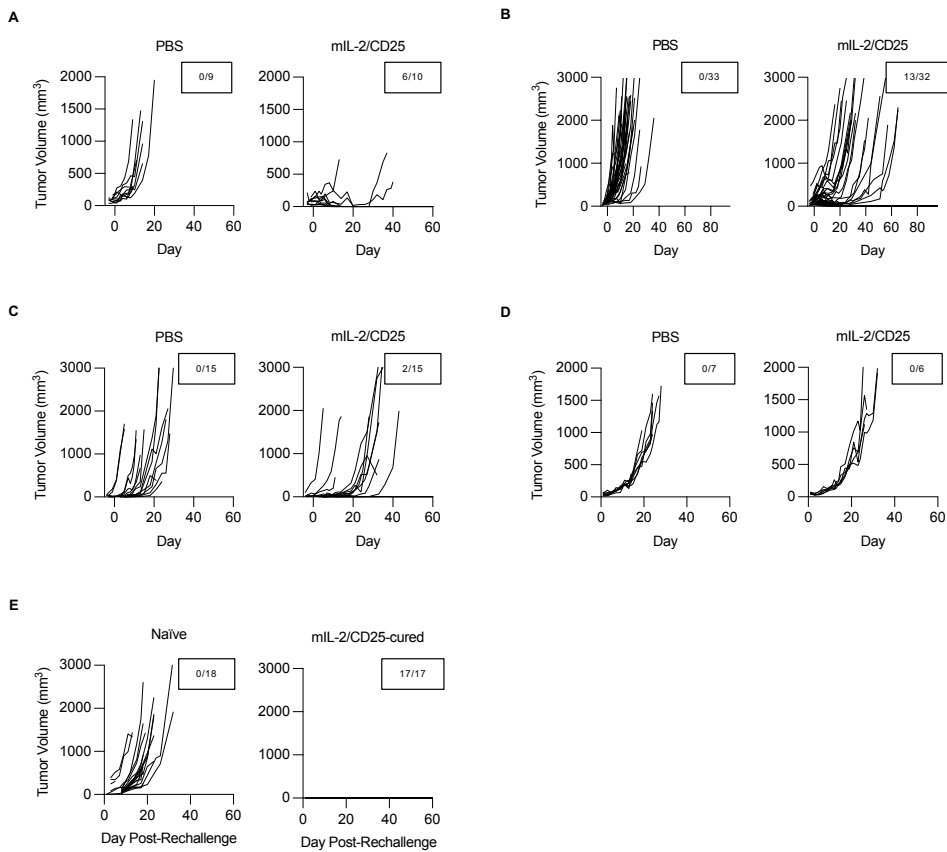
Fig. S1. HD mIL-2/CD25 delays tumor growth in immunogenic tumor models. (**A-E**) Animals were inoculated with tumors and treated as described in Fig. 1. Tumor growth curves are shown for individual animals treated with either PBS (left) or mIL-2/CD25 (right) in the (**A**) MC38 model, (**B**) CT26 model, (**C**) B16.F10 model, and (**D**) 4T1 model. (**E**) Rechallenge experiments were performed as described in Fig. 1 and tumor growth curves are shown. For all tumor growth curves, the number of surviving mice out of the total is shown. MC38 data (n=9-10/group) were pooled from 2 independent experiments. CT26 data (n=32-33/group) were pooled from 5 independent experiments. B16.F10 data (n=15/group) were pooled from 3 independent experiments. 4T1 data (n=6-7/group) were pooled from 2 independent experiments. CT26 rechallenge data (n=17-18/group) were pooled from 4 independent experiments.

Supplemental material

BMJ Publishing Group Limited (BMJ) disclaims all liability and responsibility arising from any reliance
placed on this supplemental material which has been supplied by the author(s)   *J Immunother Cancer*
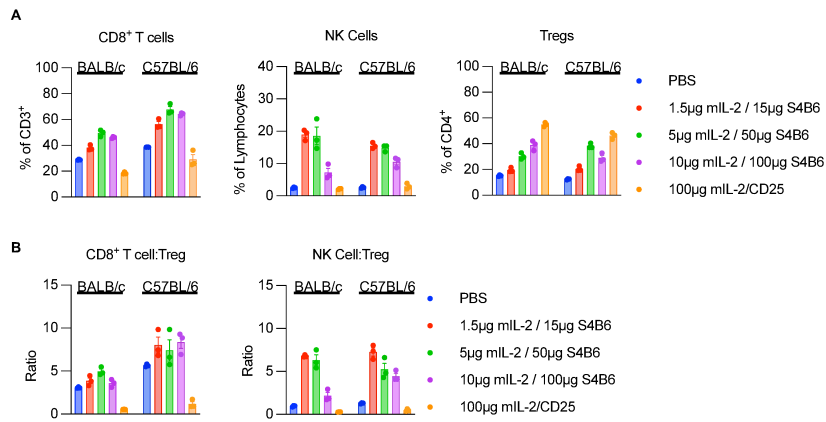
Fig. S2. The effects of different doses of S4B6-IL2/IC on CD8+ T cells, Tregs, and NK cells. (A) BALB/c and C57BL/6 mice were injected i.p. with various doses of IL-2 complexed with anti-IL-2 clone S4B6, as indicated, compared to PBS and 100 μg mIL-2/CD25. Animals were euthanized 72 hours post-injection and splenocytes were analyzed by flow cytometry. Data shows frequencies of CD8+ T cells, NK cells, and Tregs in both strains. (**B**) CD8+ T cell to Treg ratios and NK cell to Treg ratios from this experiment are shown. NK cells were defined by CD3-CD11b+Ly6G-CD49b+ in BALB/c mice and CD3-NK1.1+ in C57BL/6 mice. Data (n=3/group) are representative of 1 experiment. Error bars represent mean ± SD.

Supplemental material

BMJ Publishing Group Limited (BMJ) disclaims all liability and responsibility arising from any reliance placed on this supplemental material which has been supplied by the author(s)

J Immunother Cancer
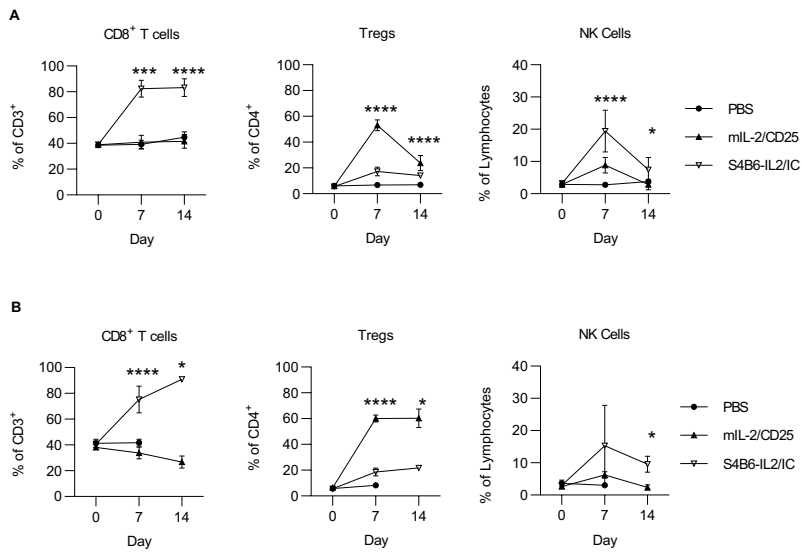
Fig. S3. Expansion of IL-2-targeted cells in the MC38 and B16.F10 models. Tumor-bearing C57BL/6 animals were treated as described in Fig. 2. (**A**) Frequencies of CD8+ T cells, Tregs, and NK cells are shown for PBMCs collected from MC38-bearing mice. (**B**) Frequencies of CD8+ T cells, Tregs, and NK cells are shown for PBMCs collected from B16.F10-bearing mice. Blood data for MC38 (n=5-9/group) and B16.F10 (n=7-8/group) were each pooled from 2 independent experiments and analyzed at each timepoint via Kruskal-Wallis test multiple comparison test. Error bars represent mean ± SD.

Supplemental material

BMJ Publishing Group Limited (BMJ) disclaims all liability and responsibility arising from any reliance placed on this supplemental material which has been supplied by the author(s)

J Immunother Cancer
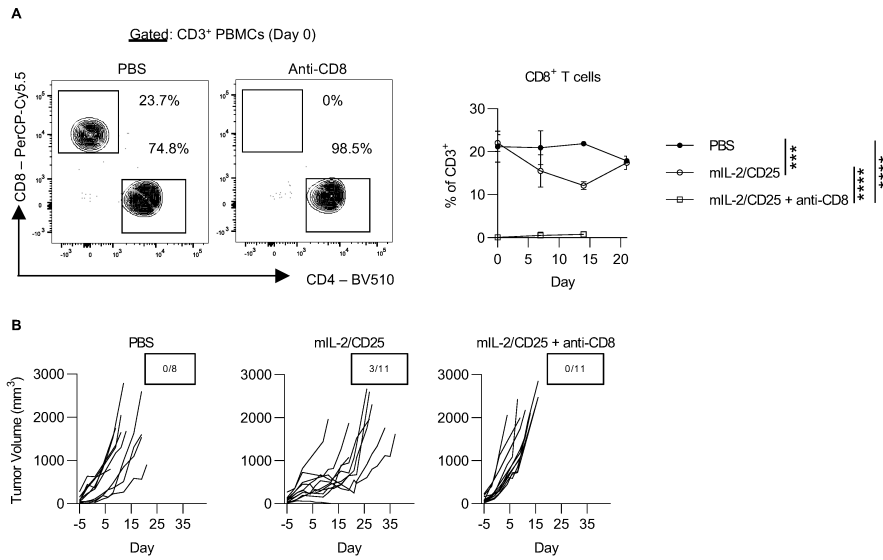
Fig. S4. CD8+ T cell depletion inhibits the mIL-2/CD25-induced antitumor response. CT26-bearing BALB/c mice were depleted of T cells and treated as described in Fig. 1. PBMCs were collected before, during, and after treatment in order to verify depletion by flow cytometry. (**A**) Data shows representative flow plots of CD4+ and CD8+ T cells after gating on CD3+ T cells in the PBMCs collected on D0. The frequency of CD8+ T cells of the CD3+ T cell population is quantified in the blood over time. Data (n=8/11/group) were analyzed via one-way ANOVA with Tukey's multiple comparison test of the AUC. Error bars represent mean ± SD. (**B**) Tumor curves are shown for the depletion experiments.

Supplemental material

BMJ Publishing Group Limited (BMJ) disclaims all liability and responsibility arising from any reliance placed on this supplemental material which has been supplied by the author(s)

J Immunother Cancer
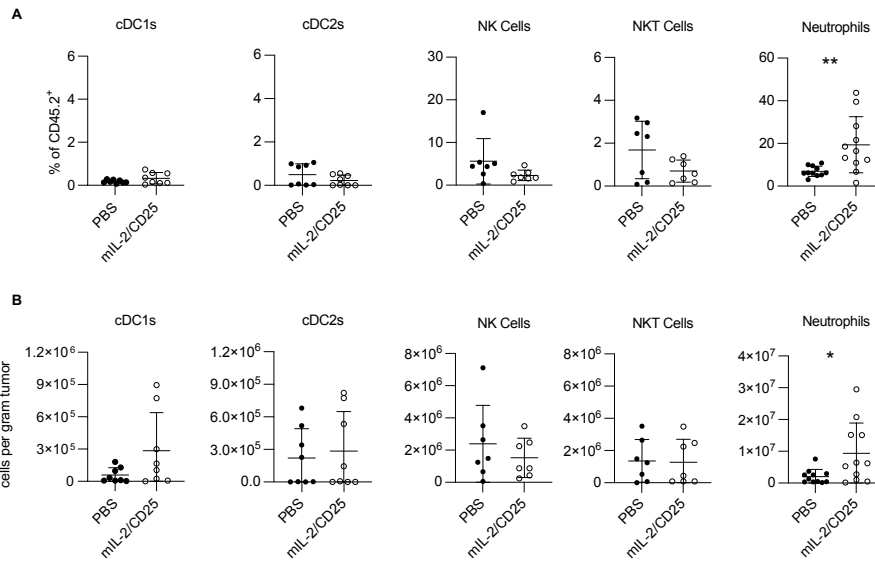
Fig. S5. The antitumor effects of mIL-2/CD25 do not act significantly through the non-T cell compartment. (**A-B**) The CT26 TME was analyzed as described in Fig. 3. Frequencies (**A**) out of the total tumor-associated immune population (CD45.2$^+$) and cell numbers per gram tumor (**B**) are shown. Type 1 conventional dendritic cells (cDC1s) were defined as live CD45.2$^+$CD11b$^-$CD11c$^+$MHC CII$^+$CD8$^+$CD4$^-$ cells. Type 2 conventional dendritic cells (cDC2s) were defined as live CD45.2$^+$CD11b$^-$CD11c$^+$MHC CII$^+$CD8$^-$CD4$^+$ cells. NK cells were defined as live CD45.2$^+$CD3$^-$CD11b$^+$Ly6G$^-$CD49b$^+$ cells. NKT cells were defined as live CD45.2$^+$CD3$^+$CD11b$^+$Ly6G$^-$CD49b$^+$ cells. Neutrophils are defined as live CD45.2$^+$CD3$^-$CD11b$^+$Ly6G$^+$CD49b$^-$ cells. Data (n=7-11/group) were pooled from 3 experiments and analyzed by Mann-Whitney test. Error bars represent mean ± SD.

Supplemental material

BMJ Publishing Group Limited (BMJ) disclaims all liability and responsibility arising from any reliance placed on this supplemental material which has been supplied by the author(s)

J Immunother Cancer
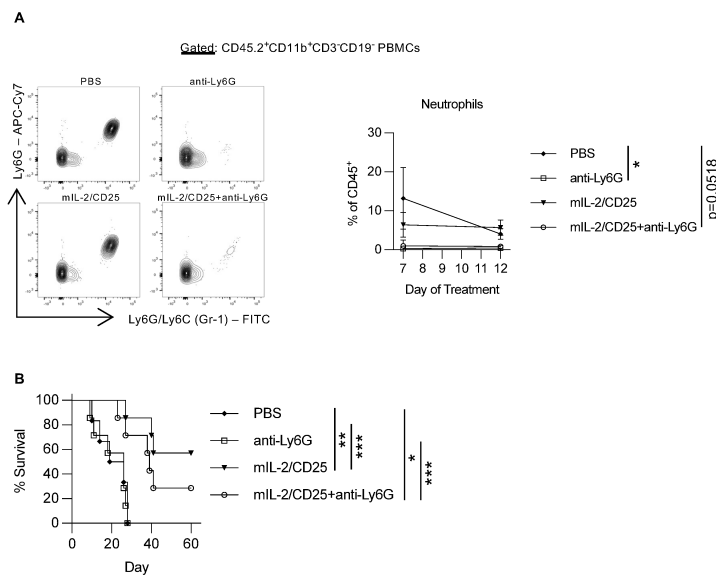
Fig. S6. Verification of Neutrophil depletion during therapy. CT26-bearing animals were depleted of Neutrophils via anti-Ly6G clone 1A8 throughout therapy. (**A**) Representative flow plots show both Ly6G and Gr-1 staining of PBMCs collected on D7 and the frequency of Neutrophils (Ly6G+CD11b+CD3-CD19-) of the CD45.2+ immune compartment is shown for D7 and D12 PBMCs. (**B**) Mouse survival is shown. Data (n=6-7/group) were pooled from 2 independent experiments. Blood data (n=5-7/group) was analyzed as a one-way ANOVA with Tukey's multiple comparison test of the AUC. Survival data were analyzed via a Log Rank test. Error bars represent mean ± SD.
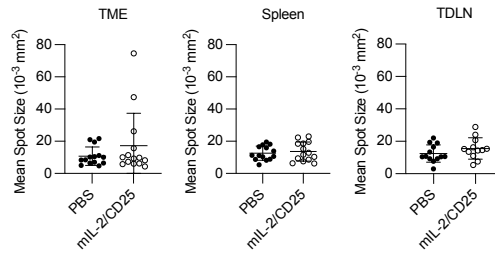
Fig. S7. HD mIL-2/CD25 does not increase the levels of IFNγ made on a per CD8+ T cellular basis. Mean spot size is shown for the IFNγ ELISpot experiments from Fig. 5. ELISpot data (n=12-14/group) were pooled from 5 independent experiments and analyzed by Mann-Whitney test. Error bars represent mean ± SD.
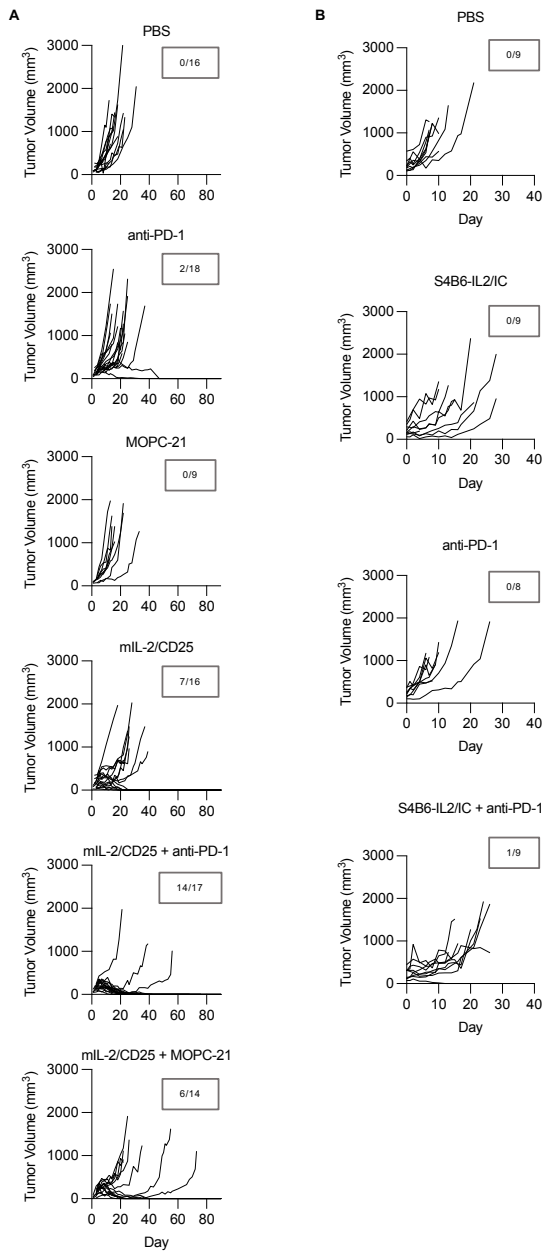
Fig. S8. HD mIL-2/CD25 combined with PD-1 blockade supports higher inhibition of tumor progression. (**A**) Tumor growth is shown for the mIL-2/CD25 and anti-PD-1 experiments in Fig 7A. (**B**) Tumor growth is shown for the S4B6-IL2/IC and anti-PD-1 experiment in Fig 7C.

Supplementary Table 1. List of fluorochrome-labeled, biotin-labeled monoclonal antibodies, and fluorochrome-streptavidin conjugates used for flow cytometry in this study, along with source and staining concentration.

| Antigen	Clone	Fluorophore	Concentration	Company	Cat. No.
CD45.2	104	APC	1:100	BioLegend	109814
CD45.2	104	APC-Cy7	1:100	Invitrogen	10-0454-81
CD45.2	104	Biotin	1:100	BD Biosciences	558702
CD3	17A2	AlexaFluor700	1:100	Invitrogen	56-0032-82
CD3	17A2	BV750	1:100	BioLegend	100249
CD3	145-2C11	FITC	1:150	Invitrogen	11-0031-82
CD4	RM4-5	BV510	1:100	BioLegend	100553
CD8α	53-6.7	Alexa Fluor 700	1:100	Invitrogen	56-0081-82
CD8α	53-6.7	BV605	1:100	BioLegend	100744
CD8α	53-6.7	BV650	1:100	BioLegend	100742
CD8α	KT15	FITC	1:100	Invitrogen	MA5-16759
CD8α	53-6.7	PerCP-Cy5.5	1:100	BioLegend	100734
CD44	IM7	Pacific Blue	1:50	BioLegend	103020
CD44	IM7	PE	1:300	Invitrogen	12-0441-83
CD44	IM7	Alexa Fluor 700	1:100	BioLegend	103026
CD44	IM7	APC-Cy7	1:100	BioLegend	103028
CD25	PC61	BV605	1:100	BioLegend	103036
CD25	3C7	PE	1:100	BioLegend	101904

Supplemental material

BMJ Publishing Group Limited (BMJ) disclaims all liability and responsibility arising from any reliance placed on this supplemental material which has been supplied by the author(s)

J Immunother Cancer

CD25	PC61	PE-Cy7	1:100	BioLegend	102016
CD25	PC61	PE-Texas Red	1:100	BioLegend	102048
CD11b	M1/70	FITC	1:100	Invitrogen	11-0112-41
CD11b	M1/70	BV650	1:100	BioLegend	101259
CD11c	N418	BV605	1:100	BioLegend	117333
CD19	ID3	BV711	1:200	BD Biosciences	563157
CD19	6D5	PE/Dazzle 594	1:200	BioLegend	115554
CD49b	DX5	PE-Cy7	1:50	BioLegend	108922
Ly6C	AL-21	Biotin	1:500	BD Biosciences	557359
Ly6G	1A8	APC-Cy7	1:100	BioLegend	127624
Gr-1	RB6-8C5	FITC	1:100	BioLegend	108406
MHC CII (I-A/I-E)	M5/114.15.2	PerCP-Cy5.5	1:200	BioLegend	107626
NK1.1	PK136	PE	1:100	BioLegend	108708
PD-1 (CD279)	J43	BV421	1:50	BD Biosciences	565942
PD-1 (CD279)	RMP1-14	PE	1:100	BioLegend	114118
PD-1 (CD279)	RMP1-30	Biotin	1:100	BioLegend	109106
LAG-3 (CD223)	C9B7W	PerCP-Cy5.5	1:40	BD Biosciences	564673
Streptavidin	N/A	BV605	1:100	BioLegend	405229
Streptavidin	N/A	PE-CF594	1:100	BD Biosciences	562284
Streptavidin	N/A	PE-Cy7	1:100	Invitrogen	25-4317-82

Supplemental material

BMJ Publishing Group Limited (BMJ) disclaims all liability and responsibility arising from any reliance placed on this supplemental material which has been supplied by the author(s)

J Immunother Cancer

Foxp3	FJK-16s	eFluor 450	1:200	Invitrogen	48-5773-82
Foxp3	FJK-16s	PerCP-Cy5.5	1:100	Invitrogen	45-5773-82
Foxp3	FJK-16s	PE-Cy7	1:100	Invitrogen	25-5773-82
Foxp3	FJK-16s	Alexa Fluor 488	1:100	Invitrogen	53-5773-82
Ki67	B56	Alexa Fluor 700	1:50	BD Biosciences	561277
TOX	TXRX10	eFluor 660	1:40	Invitrogen	50-6502-82
TCF1	S33-966	PE	1:50	BD Biosciences	564217
Granzyme B	GB11	Alexa Fluor 647	1:50	BD Biosciences	560212
TNFα	MP6-XT22	PerCP-Cy5.5	1:100	BioLegend	506322
IL-2	JES6-5H4	PE-Cy7	1:20	Invitrogen	25-7021-82
IL-2	JES6-5H4	PE	1:100	BioLegend	503808
IFNγ	XMG1.2	PE/Dazzle 594	1:100	BioLegend	505846
Fixable Viability Dye	N/A	eFluor 455UV	1:100	Invitrogen	65-0868-18
Fixable Viability Stain	N/A	440UV	1:100	BD Biosciences	566332
AH1 Tet	N/A	APC	1:150	N/A	N/A
AH1 Tet	N/A	BV421	1:150	N/A	N/A
Neg control Tet	N/A	PE	1:150	N/A	N/A

3